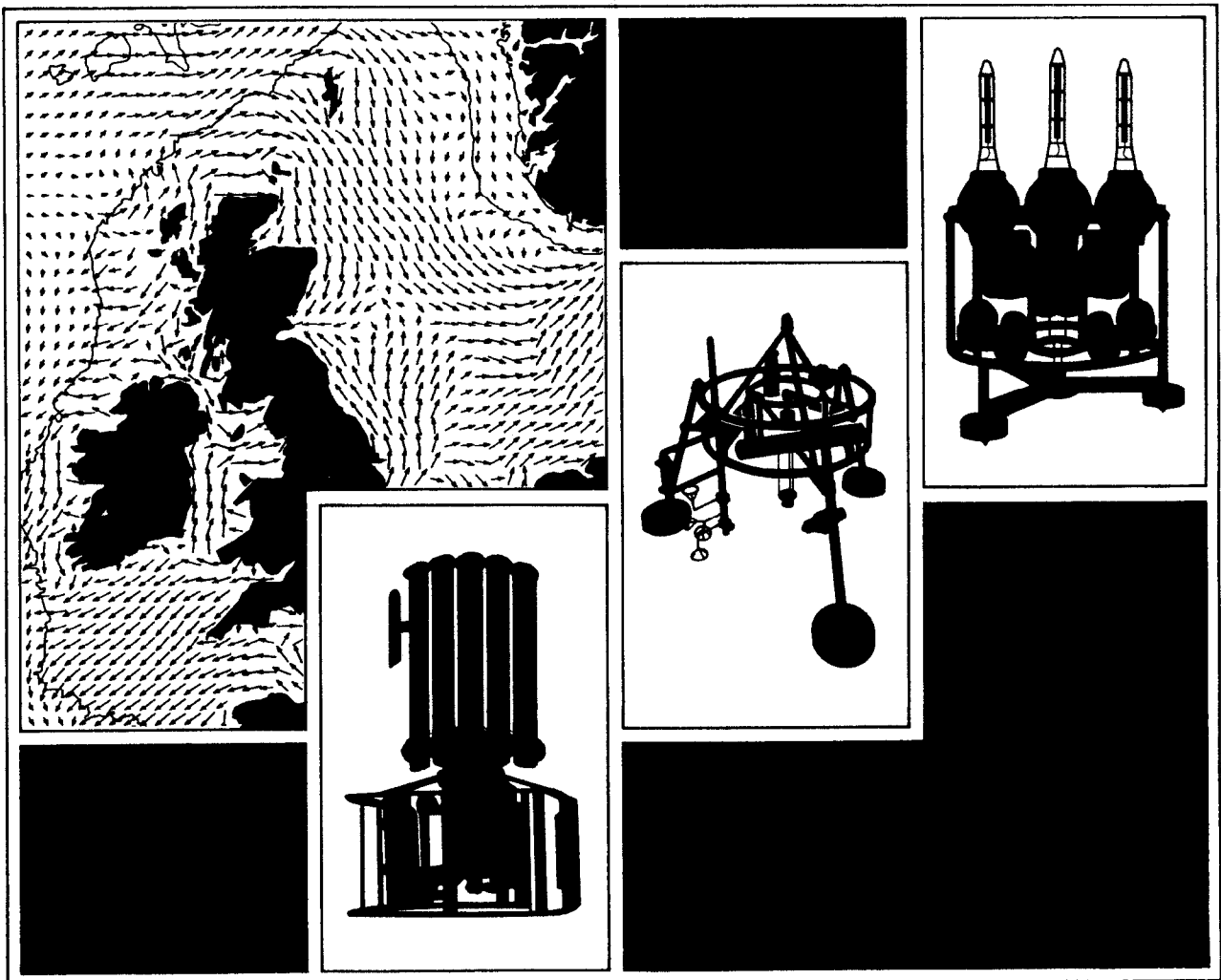# Remote Sensing Applied to Operational Models -
North Sea

AD Jenkins  G Evensen  E Bjørgo  H Espedal  E Korsbakken  K Kloster
T Hamre  V Jensen  P Samuel  D Durand  M Gómez Lahoz
J Carlos Carretero  C de Valk  K Mastenbroek  RJ Vos  H Gerritsen
and PGJ ten Brummelhuis
Report No. 49 1997

# PROUDMAN OCEANOGRAPHIC LABORATORY

**Bidston Observatory**
**Birkenhead, Merseyside, L43 7RA, UK**
**Tel: 0151 653 8633**
**Telex: 628591 Ocean B**
**Fax: 0151 653 6269**

Director: Dr. B.S. McCartney

PROUDMAN OCEANOGRAPHIC LABORATORY

REPORT NO. 49

# Remote Sensing Applied to Operational Models – North Sea

Alastair D. Jenkins, Geir Evensen, Einar Bjørgo, Heidi Espedal,
Erik Korsbakken, Kjell Kloster, Torill Hamre, Vibeke Jensen,
Paul Samuel, Dominique Durand
Nansen Environmental & Remote Sensing Center (NERSC), Bergen, Norway

Marti Gómez Lahoz & Juan Carlos Carretero
Clima Marítimo, Madrid, Spain

Cees de Valk & Kees Mastenbroek
ARGOSS BV, Vollenhove, The Netherlands

Robert J. Vos, Herman Gerritsen & Paul G. J. ten Brummelhuis
Delft Hydraulics, The Netherlands

1997

# DOCUMENT DATA SHEET

**TITLE**

Remote Sensing Applied to Operational Models – North Sea.

**REFERENCE**

Proudman Oceanographic Laboratory, Report No. 49, 55pp & Appendices.

**ABSTRACT**

This report is a review of the availability of remote sensing data, principally from satellites, for application to pre-operatioal modelling at a North Sea scale. Such data cover the electromagnetic wave spectrum from optical wavelengths through near-infrared, thermal infrared, to microwaves, and also include radio waves of several metres wavelength if we include land-based Doppler radar instruments.

The most useful techniques are likely to be, depending on the processes which are to be monitored, and the frequency of available coverage:

*Suspended sediments and sediment transport*: Optical data, including the optical and near-infrared NOAA AVHRR channels;

*Bathymetry*: Synthetic aperture radar (SAR) for monitoring spatial and temporal variations in bottom topography;

*Waves*: Altimeter data for wave height, synthetic aperture radar (SAR) for coastal studies in areas exposed to the open ocean;

*Currents*: SAR will often show current patterns, and can be used in conjunction with infra-red images of frontal structure;

*Temperature and salinity*: Thermal infra-red images (AVHRR, ATSR), are of most value.

Satellite remote sensing data are now generally available in near-real time, so they are suitable for operational purposes via data assimilation techniques in numerical models.

*Copies of this report are available from:*
**The Library, Proudman Oceanographic Laboratory.**

# Contents

# Acknowledgements

# 1 Introduction

This report provides a review of available remote sensing data, principally from satellites, and its potential and suitability for use in operational oceanography for the North Sea. We consider the relevance of the data in particular to numerical modelling activities in the coastal zone and shelf seas: both pre-operational and fully operational models. Although the MAST-III project 'PROMISE', within which this report was prepared, focuses on modelling relevant to coastal sediment transport, it is not restricted to that topic, and so we cover the application of remote sensing in more general terms. Appendix A covers the particular application of currently available remote sensing data to sediment transport.

The survey and the protection of these areas, of such great economic value, requires comprehensive knowledge, forecasting capability, and the ability to assess environmental impacts. Because of its situation, the coastal zone is one of the most sensitive regions. Terrestrial discharge, oil spills, toxic phytoplankton blooms, and coastal erosion, are examples of the kinds of processes and incidents which take place, with great consequences for human health, economic activities, and the local, regional, and global environment. Near the shorelines, investigation and measurements present some difficulties as shallow waters limit access for traditional field surveys.

Considerable economic and social benefits are expected from operational services as numerical coupled forecast models improve, partly due to more frequent and higher quality remote sensing data and advanced assimilation techniques. This will benefit and increase safety for the merchant fleet, and the fishing, offshore, and aquaculture industries. It will also assist coastal zone management, provide early warning of floods, protect the marine environment and improve monitoring of large-scale climate change (Woods et al., 1996).

**Models:** Pre-operational models are routinely used to supply information in statistical or time-series format pertaining to specific locations and time intervals for policy development, management options, engineering designs and in associated scientific research studies. Fully operational models are required for real-time forecasts of flood levels, oil spill tracks, ship routing, and for the operation of storm-surge barriers in the Thames and near the mouths of the Rhine. Also, harbour traffic control systems require real-time forecasts of wave heights and tide levels for optimal use of dredged access channels. In the future, reliable forecast systems will be required for applications such as the management of ecologically sensitive areas. Validation, and assimilation of field measurements and remote sensing observations, will be a major step in the development of fully operational models. Pre-operational modelling in oceanography shares the analogous need with meteorology for internationally organized monitoring and communications networks and for rationalisation of the range of models used.

**PROMISE project:** The PROMISE project focuses on coupling of different physical processes on different time scales, coupling models with observational data and coupling

of expertise and existing models at eleven European instututes: Proudman Oceanographic Laboratory, Birkenhead, U.K. (POL); University of Hamburg, Institut für Meereskunde; Hydromod, 22880 Wedel, Germany; GKSS, 21502 Geesthacht, Germany; Delft Hydraulics, Delft, The Netherlands; Argoss BV, Vollenhove, The Netherlands; University of Lille, France; Katholieke Universiteit Leuven, Belgium; Management Unit of the North Sea Mathematical Models (MUMM), Brussels, Belgium; Clima Marítimo - Puertos del Estado, Madrid, Spain; and Nansen Environmental and Remote Sensing Center (NERSC), Bergen, Norway.

**Remote sensing applications:** Remote sensing techniques have over the last two decades matured to such a stage that "quality" products of ocean wind, waves, temperature, eddy and frontal location and propagation and water quality can be produced routinely (Ikeda and Dobson, 1995). However, so far the most frequent variables retrieved from satellite sensors used in national and international pre-operational and operational systems are wind, waves, temperature and ice conditions. Fig. 1 gives a summary of which geophysical features and processes can be observed with different remote sensing techniques available today.

Supplementing *in situ* observations with remote sensing data will greatly add to their value, particularly in monitoring ocean wave, wind, and current fields in the coastal areas considered. The natural variability of marine parameters which can be observed using satellite remote sensing techniques means that the near-real-time acquisition of satellite data will be very important in coastal monitoring applications.

In the following sections, we consider firstly the oceanographic parameters required for operational modelling and how remote sensing information could be used to determine or increase their accuracy, timeliness and/or usefulness; and secondly we look at the types of remote sensing data available in more detail, classifying it in terms of the wavelength or frequency in the electromagnetic-wave spectrum.

We also attach three appendices, detailing:

A Verification of the WAM wave model with respect to satellite radar altimeter data from TOPEX/POSEIDON, for the Bay of Biscay and surrounding regions of the north Atlantic;

B The use of NOAA/AVHRR satellite remote sensing data for modelling suspended sediment transport in the North Sea; and

C Data assimilation for developing and implementing operational marine monitoring and prediction systems for the European coastal zone, i.e. in a EUROGOOS framework.
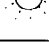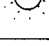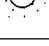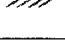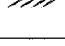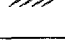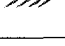
| I. Geophysical variables and features | Satellite surface remote sensing monitoring by | | | | | |
| --- | --- | --- | --- | --- | --- | --- |
| | Visible Near IR | Thermal IR | Passive MW | SAR | RA | Scatt. |
| Temperature fronts | | ○ | | | | |
| Current fronts | ○ | | | ● | ● | |
| Mesoscale eddies | ○ | ○ | | ● | ● | |
| Upwelling | ○ | ○ | | ● | | |
| Wind fronts | | | | ● | | |
| Wind speed | | | ● | ● | ● | ● |
| Wind direction | | | | ● | | ● |
| Surface waves | | | | ● | ● | |
| Internal waves | | | | ● | | |
| **II. Water quality** | | | | | | |
| Algae blooms | ○ | | | | | |
| Surfactants | ○ | | | ● | | |
| Oil spills | ○ | ○ | | ● | | |
| Turbidity & sediments | ○ | | | | | |
| **III. Sea ice parameters** | | | | | | |
| Ice concentration | ○ | | ● | ● | | |
| Ice types | | | ● | ● | | ● |
| Ice motion | ○ | | | ● | | |
| Ice edge | ○ | ○ | ● | ● | ● | ● |

○ Cloud-free and/or daylight dependent   ● Cloud and daylight independent

Fig. 1: Geophysical oceanographic features and processes observed by remote sensing techniques. Adapted from Johannessen et al. (1993).

# 2  Data required for operational modelling

To monitor key relevant parameters, a wide range of different satellite systems and sensors is and will be available. Large-, regional- and meso-scale weather and ocean features can be monitored by polar orbiting satellites with sensors operating in a wide part of the spectrum. Microwave sensors aquire data independent of sunlight and clouds, and are used to monitor wind, waves, ocean currents, oil spills, and sea ice. Visible and infra-red (IR) sensors (NOAA AVHRR, MOS (DLR) on IRS-P3 (Indian satellite) and MIR (Russian)) monitor sea surface temperature, fronts, currents, eddies and ocean colour. Small-scale features such as oil slicks, nearshore circulation and wave fields, can, under favourable meteorological conditions (normally the wind speed must be in the range 3–11 m/s) can, be monitored with high-resolution polar orbiting radar sensors.

## 2.1  Temperature and salinity

The sea surface temperature (SST) embodies significant information related to wide range of marine environmental issues. The SST variation may be related to the presence of water bodies of different origin, this implies that information related to ocean currents, fronts, meso-scale eddies and up-welling phenomenon are revealed by this type of data.

This opens up applications of satellite derived SST information in coastal mapping (Johannessen and Mork, 1979; Johannessen et al., 1993) and regional ocean circulation (Johannessen and Mork, 1979; Johannessen et al., 1993; Johannessen, 1986; Bijlsma et al., 1991), fisheries (Pettersson, 1990), algal blooms (Johannessen et al., 1989; Dundas et al., 1989), including data assimilation in physical circulation models (Stanev, 1994). Sea-surface temperatures can be monitored by thermal infra-red imagery, during cloud-free conditions, using the thermal infrared channels of the NOAA AVHRR (Advanced Very High-Resolution Radiometer) and from the ERS ATSR (Along Track Scanning Radiometer) sensor systems. These provide information on the sea surface temperature distribution at a spatial resolution of 1 km and an accuracy of 0.2°C (NOAA, 1995). The structure of meso-scale ocean circulation features in e.g. the North Sea tidal front and the Norwegian coastal current were early documented through use of this type of Earth observation data.

Passive microwave imagery can also be used to determine SST, but at a North Sea scale the available resolution is rather poor, and data reduction is rather difficult. There is a possibility for determining salinity by the use of multiple-wavelength passive microwave radiometry, but airborne sensors are required, as the resolution of satellite-borne instruments is inadequate.

## 2.2  Sea-surface elevation

Information on sea-surface elevation is important for predicting tides and storm surges. This can be obtained from radar altimetry, but detailed information on the satellite orbit is required. Such information can be obtained for the purposes of tidal analysis, but is not

generally available soon enough in order for near-real-time assimilation into storm-surge prediction models. In the absence of a sufficiently accurate geoid model, altimetry can only provide information of the variable part of the topography due to ocean dynamics, but this variability can be related to the eddy kinetic energy of the surface circulation (Samuel et al., 1994). In order to resolve mesoscale features at high latitudes, the altimeter ground track should have a cross-track spacing of the order of a few tens of kilometres and a repeat period of a few days. This will be possible only if two or more satellites carrying altimeters are flown simultaneously. Also, for coastal applications, improvements in the antenna tracking mechanism are necessary to prevent loss of data when the ground track crosses over from land to sea.

## 2.3 Currents

At a North Sea scale, these consist of tidal currents, currents driven by sea-surface gradients, and those driven by density differences. In addition, rapidly-spatially-varying currents exist near coasts and in areas of shallow bathymetry. Sea temperature fronts and the locations of their associated currents can be identified in thermal infra-red images.

Nearshore surface current fields can be determined by the use of land-based Doppler HF radar (Crombie, 1955; Lipa and Barrick, 1986; Andersen and Smith, 1989; Prandle, 1991; Shay et al., 1993), and some studies have also indicated that it is possible to monitor currents out of sight of land, using ionospheric reflections (Georges et al., 1996).

Synthetic aperture radar (SAR) is able to image the surface expressions of features such as eddies, meanders, fronts and jets, thereby providing qualitative information on their structure and evolution (Lyzenga, 1991; Johannessen et al., 1991; Johannesen et al., 1994). Products that may be considered for operational use include manually interpreted images and geographical co-ordinates of the relevant observed features.

Even though SAR is capable of seeing through clouds and in the absence of daylight, it is unable to image circulation features at very low or high wind speeds, and its capability can also be degraded in the presence of heavy rain. Since these circulation features frequently also have an expression in the surface temperature (see Fig. 2 and Johannessen et al. (1996d)) and ocean colour field, they may be detectable by visible and infra-red radiometers under cloud-free and/or daylight conditions. Thus, products combining information from these different types of sensors will be useful under varied environmental conditions and therefore more suited for operational use.

Although circulation features can be imaged by SAR, it is not generally possible to make a good quantitative estimate of the magnitudes of the currents involved, although a number of numerical models exist which aim to at least predict the radar backscatter variations produced in association with various types of surface current pattern, e.g. oceanic fronts, internal waves etc. Interferometric SAR is able, under suitable circumstances, of giving direct quantitative measurements of surface currents (Shemer, 1993; Graber et al., 1996), but is at present only deployed on aircraft.

The use of satellite altimetry to determine geostrophic currents by means of measuring sea-surface elevation gradients is limited by the available accuracy in orbit determination.

a  3°E          4°E          b  3°E          4°E

61°N

61°N

60°N

60°N

59°N

59°N

AZ

5°E          © ESA/TSS          5°E
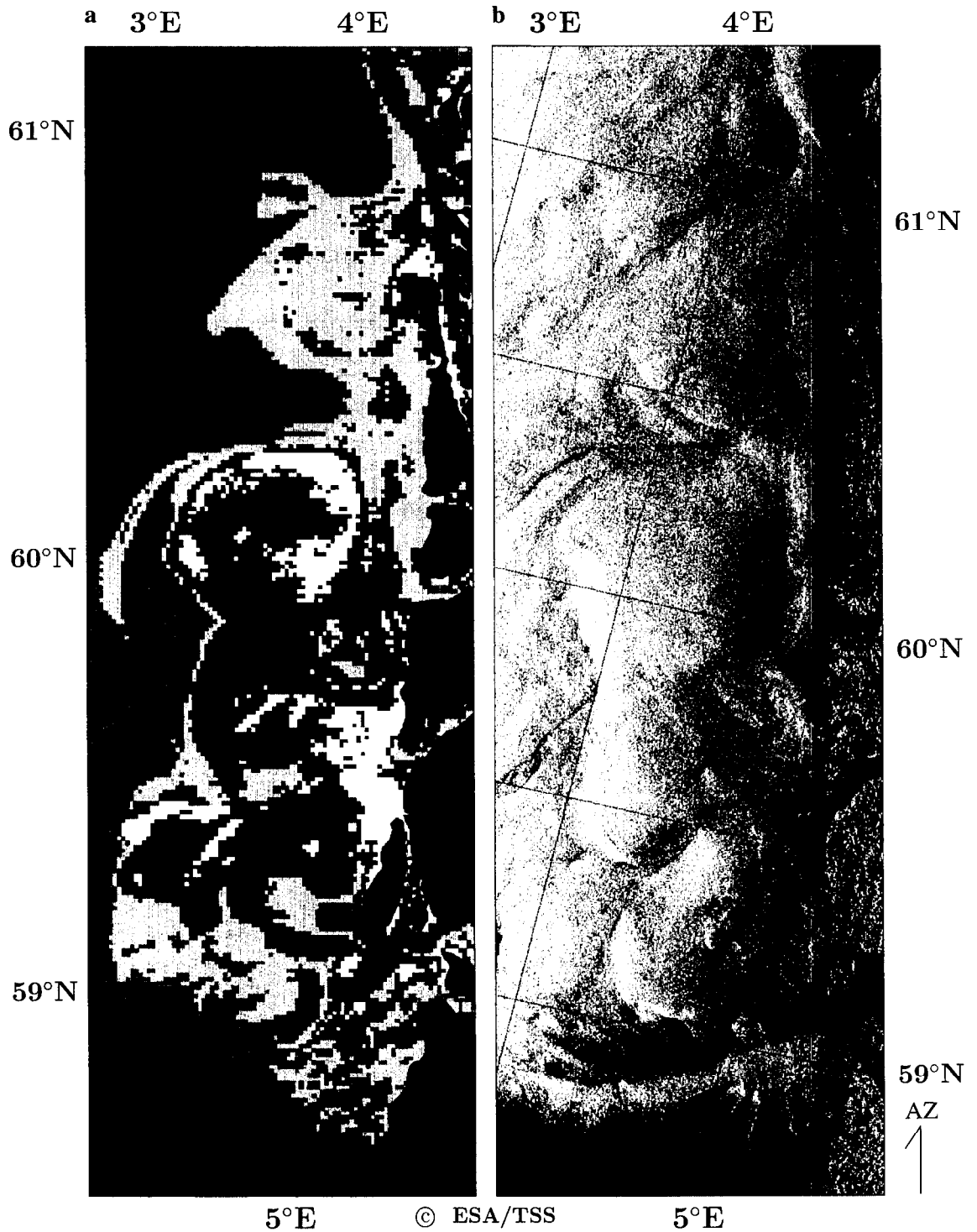
Fig. 2: Expressions of the Norwegian Coastal Current front on October 3, 1992 in a NOAA AVHRR image at 1420 UTC (left) and a SAR image ©ESA/TSS 1995 acquired at 2135 UTC. Both images cover the same 100 km × 300 km region. From Johannessen et al. (1996a).
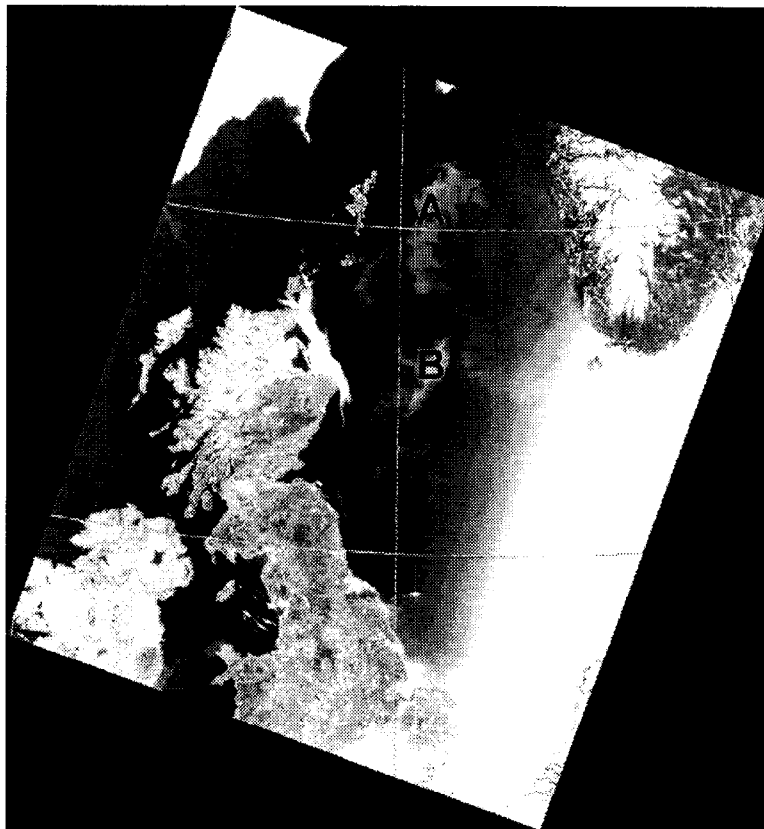
Fig. 3: NOAA AVHRR channel 1 (visible) image of 1995 June 27, from the North Sea, showing two coccolithophorid blooms east of respectively Shetland (A) and Scotland (B). The blooms cover areas of 22 000 and 7 500 km$^2$ respectively. After Pettersson (1995).

In the absence of such detailed orbit information, it is still possible to obtain an estimate of the eddy kinetic energy of the circulation, from the measured gradients.

## 2.4 Wind

Wind speed and direction are determined on a routine basis from the radar scatterometer on the ERS-2 satellite. It is also possible to determine detailed patterns of wind speed, and sometimes direction, from synthetic aperture radar (SAR) images, and, at a lower resolution, from real-aperture satellite side-looking radar instruments. Satellite altimeter data can also be used to determine wind speed along the orbit (Witter and Chelton, 1991; Carter et al., 1992; Monaldo, 1988).

### Wind retrievals

Scatterometer observations over the ocean provide direct estimates of the global wind vector field at spatial resolution of 50 km with an accuracy of 2 m/s in speed, 15° in direction, but usually with a directional ambiguity of 180°. For some applications, such as in semi-enclosed seas, in straits, in coastal regions, and in estuaries, this resolution is, however, too coarse. In these regions, wind field estimates retrieved from high resolution SAR images can be very useful. Today, SAR is the only satellite borne instrument that can provide high spatial resolution images ($\approx 30 \times 30$ m ground resolution) of the ocean surface for visualization and spatial resolution down to $10 \times 10$ km for quantitative measurements of mesoscale wind field. The spatial coverage is $100 \times 100$ km which is the ERS SAR image size.

### Wind retrieval algorithms

Fig. 4 shows a conceptual overview of the wind field estimation as further described below.

### SAR Wind Algorithm

The SAR Wind Algorithm (SWA) proposed by Vachon and Dobson (1996) and further examined by Chapron et al. (1995) and Kerbaol et al. (1996) is based on a relation between the smearing effects (Hasselmann and Shemdin, 1982) in the SAR image and the wind field. Smearing effects tend to increase the coherence (correlation) length of the radar returns in the spatial image domain and influence on the spectral properties of the SAR image. In case of a fully developed sea (no fetch limitation) the empirical relation, based on evaluation of 1200 SAR wave-mode imagettes with a central incidence angle of 20.2° is given by Chapron et al. (1995) as

$$U_{10} = 4.75 \left( \frac{\lambda_c - 30}{110} \right),$$

where $U_{10}$ is the wind speed in metres per second at 10 m above the surface, and $\lambda_c$ is the azimuth cut-off wave length in metres, which can be estimated from the SAR image power spectrum.
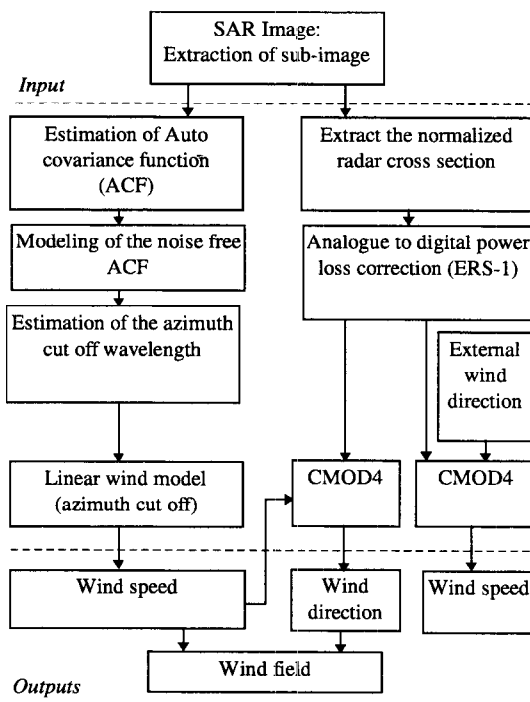
Fig. 4: Conceptual overview of wind retrieval models

## The CMOD4 model function

The CMOD4 wind retrieval model (Stoffelen and Anderson, 1993) is developed for the ERS-1 C-band[1] scatterometer but it is also shown to give good estimates of wind speed when applied to ERS-1 SAR images (e.g. Vachon and Dobson, 1996; Johannessen et al., 1994; Vachon et al., 1995; Wackerman et al., 1995 1996). The CMOD4 empirical algorithm gives a theoretical $\sigma^0$ (normalized radar backscatter cross-section) value as a function of wind speed and direction. The accuracy in the model is $\pm 20°$ in relative wind direction and $\pm 2\,\mathrm{m/s}$ in wind speed when applied to scatterometer data. The CMOD4 model is derived for a neutral stratification. In order to compute the wind speed from the radar backscatter accounting for the stratification in the atmospheric boundary layer (ABL) the CMOD4 derived wind speed must be modified. A correction for this can be derived from expressions relating unstable and stable stratification to neutral stratification as suggested by Wu (1993) and Smith (1988). The saturation of the analogue to digital conversion (ADC) in the satellite must also be accounted for, as described by Meadows and Willis (1995), Laur et al. (1996), and Scoon et al. (1996). The effect is strongest over ocean in the near range and increases with radar backscatter intensity (i.e. at high winds) and leads to an underestimation of $\sigma^0$. For the present analysis (see also Korsbakken (1996) and Korsbakken and Johannessen (1996)), the absolute calibrated $\sigma^0$ is derived in accordance with a comprehensive calibration scheme provided by ESA (Laur et al., 1993 1996), but omitting correction for variance in the replica pulse power. The latter is shown to be negligible using the the CMOD4 algorithm for wind speed retrieval in SAR data (Scoon et al., 1996).

**Wind direction from CMOD4:** The wind direction can also be estimated from the CMOD4 model for different incidence angles provided the wind speed, derived from the SWA method, can be associated with the corresponding measured radar backscatter. In such cases four solutions, i.e. two pairs, each with a 180° ambiguity can be found, except in the cases when the direction is close to upwind (the wind blowing towards the radar) or downwind, for which only one pair is found. (Note that for the three beam scatterometer on ERS-1, 2 the number of solutions is reduced to a single pair with a 180° ambiguity) It has also been demonstrated (Johannessen et al., 1994) that wind rows manifested in SAR images can be used to indicate the near surface wind direction during the SAR integration time. In such cases the number of wind direction solution pairs is also reduced to one (180° ambiguity).

## Case studies from COAST WATCH '95

We present, as an example, a wind analysis using SAR data from the COAST WATCH '95 experiment (Johannessen et al., 1996c), carried out off the south-west coast of Norway during September 1995 (an ERS-1 / ERS-2 Tandem Announcement of Opportunity experiment).

---

[1]Radar wavelength approximately 5 cm.

The tandem operation provided an extended SAR coverage of the experiment area. Also ATSR and NOAA AVHRR data were obtained during the experiment. Meteorological and oceanographical in situ observations were provided from the research vessel R/V Håkon Mosby of the University of Bergen, and an advanced metocean buoy from the Naval Postgraduate School, Monterey.

The analysed SAR data is 3 looks ground range SAR data in ERS.PRI (SAR Precision Image) format which is corrected for antenna elevation gain and range spreading loss. The ground resolution in range (normal to satellite track) direction and azimuth is about 30 m and the pixel size is 12.5 m in each direction. All case studies are descending tracks and the nothernmost SAR image is always referred to as the first SAR image. Each SAR image (100×100 km) was divided into 81 square 11.1 × 11.1 km sub-images. The SAR image power spectrum was estimated from each sub image (cf. Monaldo, 1991), and the SWA wind speed was calculated. For estimation of CMOD4 wind speed and direction each sub image was averaged to a pixel size of 100×100 m before the ERS-1 data were corrected for the ADC power loss. The CMOD4 wind speed was calculated assuming the in situ wind direction to be valid in all sub images. The wind direction is estimated from the CMOD4 model function from a combination of the SWA wind speed and calibrated radar backscatter. This ambiguity is resolved by comparing the four results with the in situ measured wind direction and also the wind rows seen in the SAR image.

Figs. 5–6 show the retrieved wind fields together with isobaric maps and the surface wind results from two selected case studies from the COAST WATCH '95 experiment. The diagnostic wind field was provided by the Norwegian Meteorological Institute 90 minutes after the satellite overpass. Table 1 lists the obtained wind speeds from SWA, CMOD4, the meteorological model, and in situ measurements where available.

Surface conditions impact on the performances as fully demonstrated in the case studies. For fetch limited seas and in vicinity of wind fronts the SWA method underestimates the wind speed. For fetch limited seas the waves are not in equilibrium with the near surface wind speed. Hence, the distribution of the velocity field of surface scatters will be different than for fully developed seas and the SWA derived wind speeds are underestimated. The relaxation rate for the longer wind waves (also the medium wavelengths suppressed by the general resolution of the SAR) leads to a relatively long decay time. In cases where these waves are propagating across a wind front they will maintain their original equilibrium state over some distance away from the front. In turn, the wind front is not resolved by the SWA method, so that the azimuth smearing is strongly affected by the longer wavelengths and not the rapidly-responding wind generated short waves.

In contrast the CMOD4 method is not limited by these conditions. On the other hand, presence of long waves, mainly generated some distance away from the imaged area, and propagating into the area causes an increased SWA estimated wind speed compared to the CMOD4 derived wind speed. The combination of the SWA and the CMOD4 methods may provide a promising system for quantitative wind speed and wind direction retrievals from SAR images at high spatial resolution of 6 to 10 km but, as demonstrated in this paper, problems occur under different surface conditions. While absolute image calibration is necessary for the CMOD4 method, it is not required for the SWA method since the first
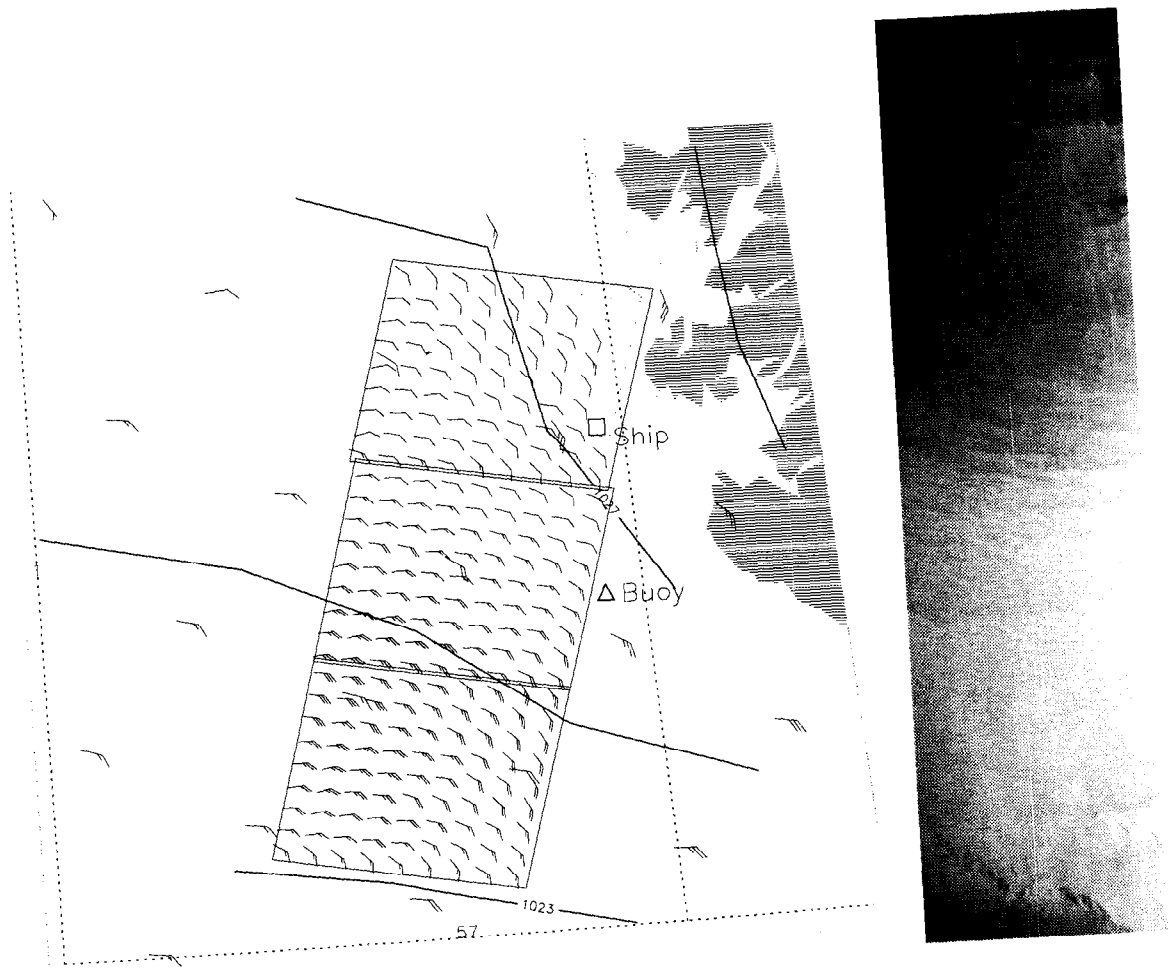
Fig. 5: Case I. Wind field derived from inverting the CMOD4 model function using the SWA wind speed and the calibrated $\sigma^0$ on 17 September 1995. The position of R/V Håkon Mosby and the metocean buoy at satellite overpass is indicated
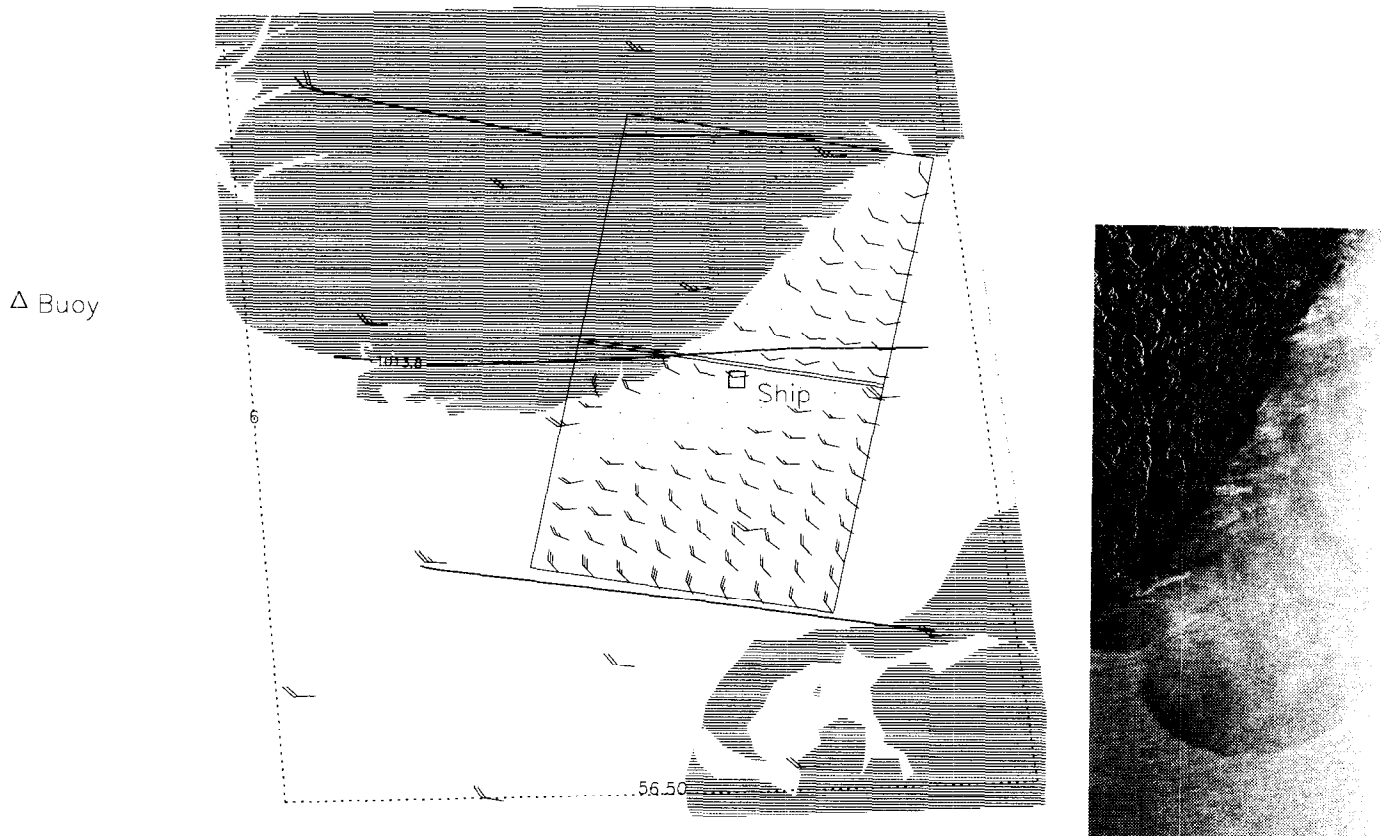
Fig. 6: Case II. Wind field from 23 September 1995.

Table 1: Comparison of wind retrieval algorithms for SAR, for the two COAST WATCH '95 case studies (Figs. 5 and 6).

| CASE I | | CASE II | |
| --- | --- | --- | --- |
| Wind speed (m/s): | Wind direction: | Wind speed (m/s): | Wind direction: |
| a) SWA | a) SWA, CMOD4 | a) SWA | a) SWA,CMOD4 |
| b) CMOD4 | b) hindcast | b) CMOD4 | b) hindcast |
| c) hindcast | c) in situ | c) hindcast | c) in situ |
| d) in situ | | d) in situ | |
| a) 4 | a) 98° | a) 9 | a) 305° |
| b) 5 | b) 124° | b) 6 | b) 262° |
| | c) 100° | c) 10 | c) 260° |
| a) 4 | a) 108° | a) 5 | a) 277° |
| b) 3 | b) 147° | b) 6 | b) 266° |
| c) 10 | c) 90° | c) 7 | |
| d) 6 | | | |
| a) 7 | a) 101° | a) 7 | a) 265° |
| b) 8 | b)124° | c) 11 | b) 261° |
| c) 8 | | | |
| a) 8 | a) 140° | | |
| b) 6 | b) 101° | | |
| c) 9 | | | |
| a) 7 | a) 87° | | |
| b) 8 | b) 96° | | |
| c) 7 | | | |

method uses radar backscatter values while the latter uses spectral characteristics.

As mentioned in the analysis of the 17 September image, the SWA method is limited to SAR images containing clear wave modulation from which the azimuth cut-off can be derived and therefore under low wind conditions (lower than approximately 3 m/s) or presence of slicks the SWA retrieved wind speed has no confidence. For the different ERS-1,2 SAR modes only the low resolution images constrain the SWA method since typical wavelengths of wind seas are not properly resolved in such images. Since future satellites such as the ENVISAT (ESA), to be launched in 1999, may not be equipped with a wind scatterometer for global wind measurements wind retrieval algorithms, as described in this paper, will become more important in the future. Table 2 lists some performance characteristics for the ERS-1,2 modes and the proposed ENVISAT ASAR (Advanced Synthetic Aperture Radar) modes. Combining improved wind field retrieval models as presented in this paper, directional ocean wave spectrum modeling Engen and Johnsen (1995), and higher order statistical analysis suggested by Chapron et al. (1995), a very advanced ocean monitoring tool to provide a wide range of information can be developed.

## 2.5 Waves

Significant wave height ($H_s$) can be determined using satellite altimeter measurements (Rufenach and Alpers, 1978; Bauer et al., 1992; Guillaume and Mognard, 1992), and such measurements have been used to validate numerical wave forecasting models (Wu et al., 1994). The use of ERS and TOPEX/Poseidon altimeter data for significant wave height in conjunction with ERS scatterometer data for wind produces encouraging improvements in wave forecast model predictions (Le Meur et al., 1996). Present operational products include assimilation of satellite altimeter derived significant wave heights into an operational regional wave forecasting model (Breivik et al., 1996), and significant improvements in the wave analysis and short-term forecasts for the North Sea were found.

A significant present use of marine remote sensing data is the use of satellite radar altimeters (ERS-1/2, TOPEX/Poseidon, Seasat, GEOS-3) to provide climatological wave height information as well as wind speed (Paci and Campbell, 1996; Lasnier et al., 1996), though it is necessary to conduct careful calibration studies for the different instruments (Carter and Cotton, 1996). The along-track resolution is typically 7 km (for ERS). These data can be used for offshore oil industry design and operational planning purposes, as well as for coastal engineering design, naval architecture, ship routing etc.

Appendix A of this report shows the application of altimeter data to the verification of waves in the Spanish coast data set.

Wave direction and wavelength can be determined using ERS SAR, both in image mode and globally in 'wave mode', and also in the high-resolution modes of Radarsat. The typical resolution of satellite SAR, about 30 m, means that only waves with periods of about 5 seconds or more can be resolved. The wave pattern visible on a SAR image may be very different from the *in situ* wave field, as well as having a 180 degree directional ambiguity, and a complex post-processing of the image is usually necessary to extract the

Table 2: Qualitative performance characteristics of the SWA and CMOD4 methods for determining wind from SAR images.
**ERS-1/2:** Data available from 1991
**Envisat:** Proposed launch date 1999.

| Characteristics | SAR wind retrieval algorithms | |
| --- | --- | --- |
| | SWA | CMOD4 |
| **ERS-1,2 SAR modes:** | | |
| Wave Mode | OK | possible[1] |
| Image Mode (SAR.PRI) | OK | OK |
| Low resolution image (100m) | not possible | OK |
| **ENVISAT ASAR Modes:** | | |
| Wave mode (near range) | OK | possible[2] |
| Wave Mode (far range) | needs to be examined | possible[2] |
| Full Image Mode (near range) | OK | OK |
| Full image mode (far range) | needs to be examined | OK |
| Wide swath (100m) | not possible | OK |
| Global Mode | not possible | OK |
| Alternating polarisation | OK | OK |

[1]The necessary information to calibrate the Wave Mode Imagettes is not provided with the standard ESA Wave Mode products.

[2]Necessary information to fully calibrate the product needs to be available

directional wave spectrum. It is usually necessary to start from an initial 'first guess' spectrum, from, say, a numerical model simulation (Hasselmann and Hasselmann, 1991; Krogstad et al., 1994). Progress in reducing the directional ambiguity and improving the signal-to-noise ratio has recently been made by employing Single Look Complex data from ERS SAR (Engen and Johnsen, 1995).

SAR does appear to give convincing images of swell waves propagating onto coasts, including the effects of depth refraction, shadowing and diffraction. The ability of SAR in image mode to provide rather detailed pictures of wave fields near shorelines, at least for the longer swell waves, should be useful in monitoring the coastal environment and its changes, including the locations of rip currents, longshore drift, and other currents which impact the transport of sediments. Wave refraction by bottom topography and the resulting change in surface roughness monitored by SAR, may be used to monitor the evolution of sandbanks in shallow-water areas, as well as in charting bathymetry in poorly-surveyed regions (Calkoen, 1996; Calkoen et al., 1991; Calkoen and Wensink, 1993; Hesselmans, 1996).

SAR wave mode data are now used to provide corrections to forecast wave directions in operational wave forecasting models, though assimilation of these data is still at a preliminary stage (Paci and Campbell, 1996; Breivik et al., 1996). The impact of these data is not very significant at present, mainly because of the sparse data coverage, but new processing techniques (e.g. Engen and Johnsen, 1995) are being evaluated and may improve the situation.

## 2.6 Turbulence

Remote sensing techniques are unlikely to be able to contribute directly to the determination of turbulence. Sources of turbulence which can be measured using remote sensing techniques include wind, waves, and currents. The effect of turbulence in suspending sediment particles can also be determined (see below).

## 2.7 Water quality

Since sea surface roughness, dissolved or suspended substances and bottom features modify the propagation of light in the water body, the study of the light field distribution provides relevant information on coastal zone biogeophysical parameters and processes. Many studies have been carried out to relate the inherent optical properties of the water to more easily measurable properties such as water-leaving radiance and vertical diffuse attenuation (Gordon et al., 1975a; Kirk, 1981). Advanced approaches take advantage of both airborne and spaceborne spectro-radiometers, and radiative transfer numerical models (RTM) (Mobley et al., 1993), to investigate and improve the understanding of coastal zone processes. Measurable parameters that can be used as input to a RTM include both *in situ* and remotely sensed measurements. Such parameters can be seen either as directly usefull variable which can be assimilated into the model or indirect parameter which require further processing

or transform in order to be assimilated. The latter includes the class of qualitative variables which somehow can be transformed into quantitative variables through empirical or semi-emprical relationships e.g. , Secchi disk, FTU turbidity.

Aspects of 'water quality' which can be observed from satellites include surface films or surfactants, algal blooms, suspended sediments and sediment transport and terrigeneous discharge. Detection, quantification, and direct or indirect monitoring of the transport and dilution of these phenomena may be performed using satellite Earth observation data in combination with other environmental information.

### 2.7.1 Natural films and oil spills

Under suitable conditions, an oil slick will dampen capillary and short gravity waves, and appear as a dark slick in a Synthetic Aperture Radar (SAR) image of the ocean surface. This effect has been used for decades in aircraft-based oil spill monitoring systems, especially in the North Sea. Now, the radar satellite ERS-2 (and soon also RADARSAT) is used in a routine satellite-based oil spill monitoring service (Fig. 7). However, this service is only based on visual interpretation of SAR images, and a number of oil spill 'look-alikes' may complicate the analysis.

To improve the performance of satellite based SAR in coastal zone oil spill detection and monitoring, a combination of model data and SAR data is preferred. Such models may include oil drift models (see Furnes, 1994) and SAR image models (Lyzenga and Bennett, 1988; Tanis et al., 1989). If a possible oil spill is detected in a SAR image, the models are used to try to reconstruct the spill (given wind, current and wave height history of the area). The discharge rate and type of oil giving the best possible match to the observed spill, is then searched. Examples are shown in Figs. 8 and 9.

### 2.7.2 Ecological aspects

The light scattering and absorbing characteristics of the phytoplankton itself and other water constituents is the basis for the use of ocean colour Earth observation sensors. The US Coastal Zone Colour Sensor (CZCS) from 1978–86 proved the usefulness of this type of Earth observation technique to map the marine chlorophyll distribution.

A number of algorithms have been developed to retrieve phytoplankton pigment concentration from ocean colour data (Morel and Prieur, 1977; Gordon et al., 1980; Prieur and Sathyendranath, 1981; Kirk, 1983; Gordon and Morel, 1983; Morel, 1988; Sathyendranath et al., 1994). Phytoplankton biomass and primary production estimation are derived from photosynthetic pigment concentration in the upper water column and Photosynthetic Available Radiation (PAR) which can be both estimated from data of spectro-radiometers measuring ocean colour. Bricaud et al. (1987); Platt and Sathyendranath (1988 1993); Sathyendranath et al. (1989). Almost all the models deal with case I oligotrophic water, as defined by Morel and Prieur (1977). Empirical or semi-empirical models relating atmosphere-corrected radiances and water constituent concentrations are used. They are based on spectral band
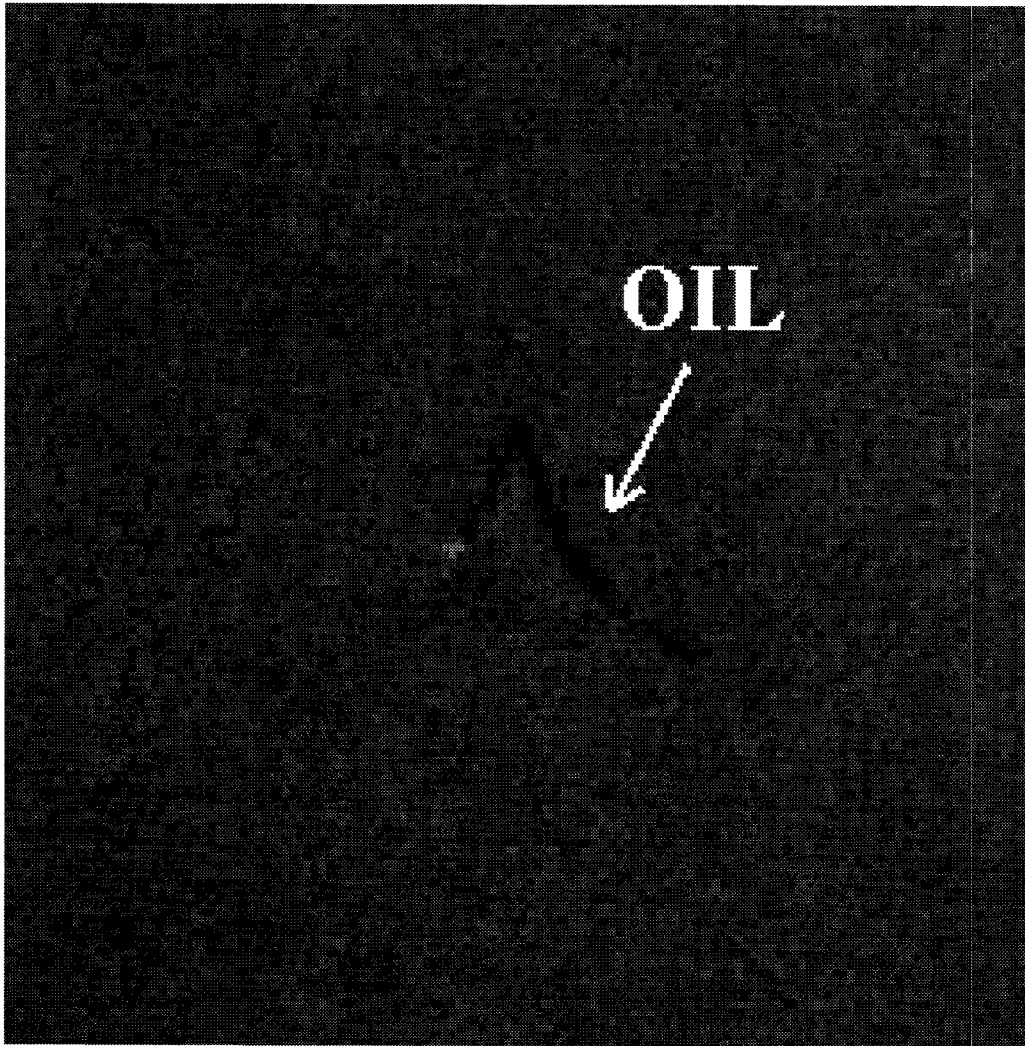
Fig. 7: An angular winding slick in an ERS-1 SAR image from 25 November 1994. The bright spot indicates the Ula platform. The spill was caused by problems with a drilling well. Such angular spills are ideal cases for input in oil drift models, given the wind and current history at the spill site.

Murchinson

Thistle

Statfjord C

Statfjord A

Dunlin

Statfjord B

Brent D

Brent C

Brent B

10km

N

0
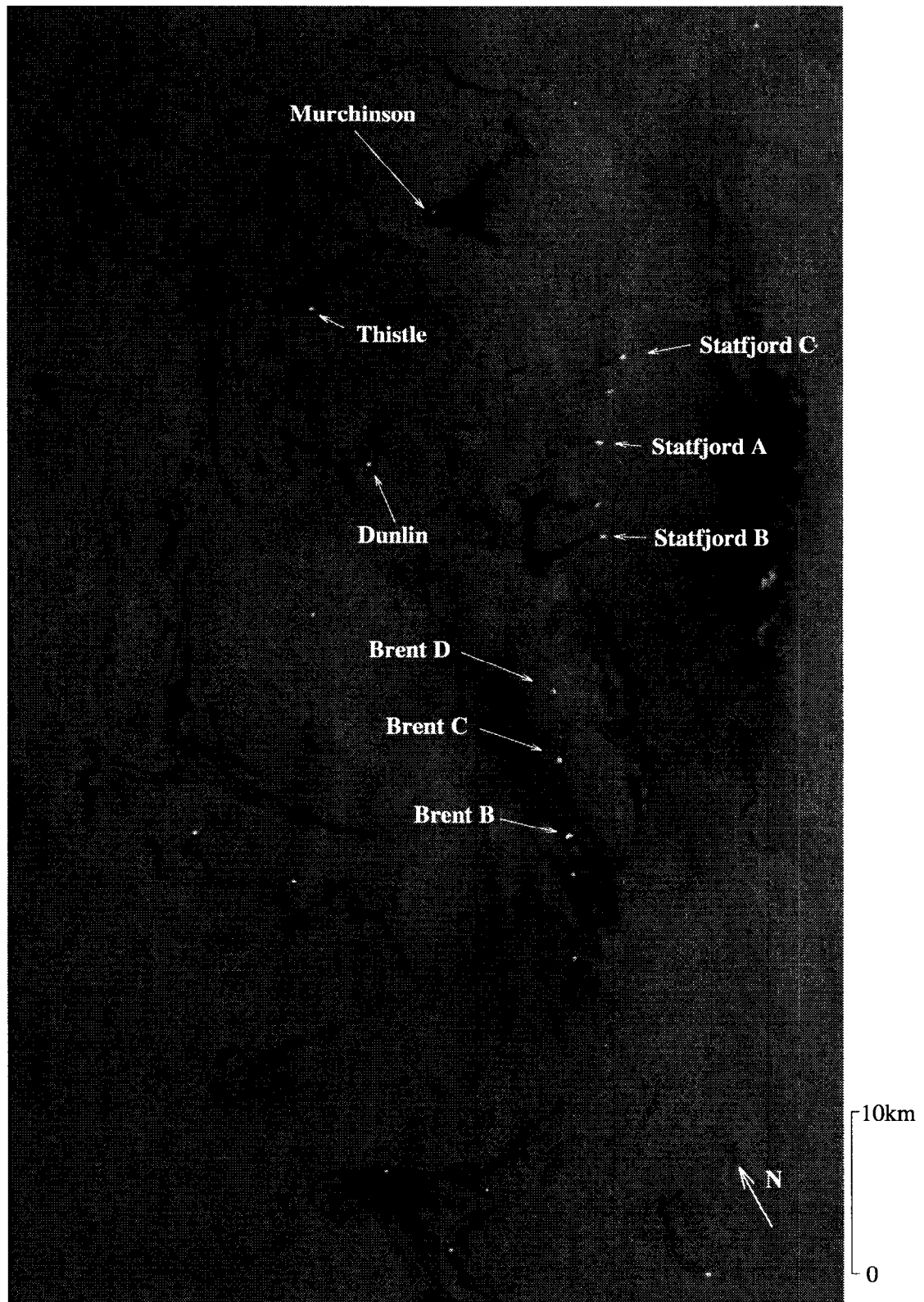
Fig. 8: This ERS-1 SAR image from 1994 October 30, contains a number of suspicious slicks, connected to or located near oil platforms in the Norwegian and British sectors in the North Sea. The angular winding slick extending from the Murchison platform is modelled using a numerical oil drift model [Furnes, 1994].
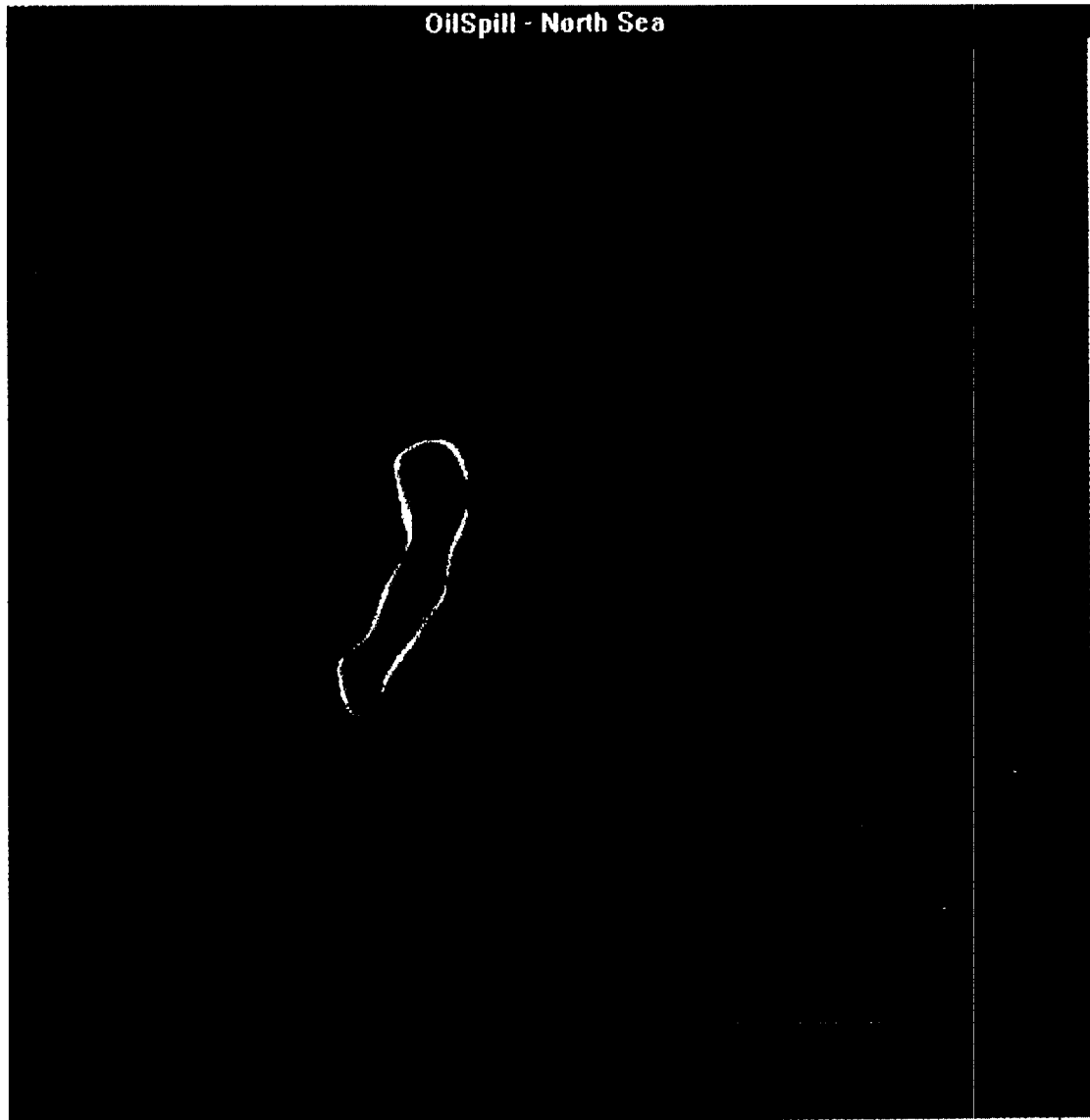
Fig. 9: The model reproduces fairly well the spill in the image of Fig. 8, but the slick has not bent completely, indicating that the spill may have occurred even before the start of the model run on October 27. A slick having survived that long on the ocean surface is very likely to contain hydrocarbons.

ratios (mainly blue/green bands) and are thus dependent upon the spectral bands characteristics of each sensor.

In the open ocean the complexity of the ocean optics is not as severe as in the coastal areas, where also the sediments and coloured dissolved organic matter (CDOM) significantly contributes to the signal measured by the satellite Earth observing sensors. Some attempts have been made to retrieve cholorphyll in case II waters e.g., Sathyendranath et al. (1987).

On the one hand, one of the main issues of surveying phytoplankton distribution and concentration is the operational monitoring of red tides and potential fishery areas (Dundas et al., 1989; Johannessen et al., 1993). The development of extreme algal blooms (harmful or not) generally depends on the following environmental conditions; (1) hydrodynamical conditions, (2) supply of macronutrients to the euphotic zone, (3) surface solar radiation, and (4) the optical properties of the water column (Johannessen et al., 1993). An algal bloom may have its peak activity sheltered below the surface, and hence may not be visible from above. The algae themselves have limited motility and hence a measure of the advection of an identified bloom may be done indirectly through monitoring of the currents and ocean circulation. An example was the extensive bloom of the toxic algae *Chrysocromulina polylepis* in the Skagerrak region in spring 1988 (Dundas et al., 1989; Aksnes et al., 1989; Johannessen et al., 1989). The bloom originated in the Skagerrak, and the algal front was subsequently advected with the warm water out of the Skagerrak region. During this event the Norwegian aquaculture industry suffered losses of the order of 3.5 MECU, while caged fish of a value of 140 MECU were towed northward and into the fresher and colder water in the fjords and saved. The monitoring efforts during this event included combined use of field observations, numerical modelling simulations and satellite and airborne remote sensing and reconnaissance.

During some events, discoloration of the water is even detectable to the human eye. An example of this is the presence of the algae *Emiliania huxleyi*, which causes a milky-white water colour during the phase when the coccoliths are formed. Such blooms are seen annually in coastal and fjord areas as well as in the open ocean, all over the world, but in particular at mid latitudes. The high reflectance of water with coccoliths make these blooms even visible in the optical channel of the AVHRR sensor (Pettersson, 1995). An example of two such blooms in the North Sea is shown in Fig. 3.

On the other hand, the estimation of primary producter biomass and production at meso and global scale are also of great interest for global and regional climate change forecsating. Such informations are needed to improve coupled physical and biogeochemical models which are used for studying carbon cycle in the atmospher/ocean system and its influence on the climate.

### 2.7.3 Suspended sediment and sediment transport

In studies of the transport of sediments, for applications to coastal erosion, changes in bathymetry, transport of deposited material, associated adsorbed pollutants,etc., it is possible to obtain a measure of suspended particle concentration from multi-channel optical and infra-red radiometer observations.

Remote sensing measurements of suspended sediment have been studied by Tassan and Sturm (1986); Tassan (1988); Curran and Novo (1988); Harwar et al. (1995) and Althuis et al. (1996). A synthesis on remote sensing measurements with respect to suspended sediment and numerical modelling has been performed recently by Xia (1993). The most advanced works in this field have been performed by Puls et al. (1994); Vos and Schuttelaar (1995).

*Beach processes and coastal erosion:* Such studies require knowledge of the wave amplitude and direction, coastal currents, bathymetry, bottom topography and the distribution of suspended sediment. These are all potentially recoverable by remote sensing, e.g. using SAR data for wave, currents, bottom topography and optical sensors for bathymetry, bottom topography and suspended sediment. Images obtained using optical and infra-red spectrometers and radiometers are potentially capable of retrieving bathymetry (Mishra et al., 1989; Bijaoui et al., 1994; Polcyn and Sattinger, 1969; Bierwirth et al., 1993), bottom type (Estep and Holloway, 1992; Estep, 1994; Lyzenga, 1978 1981) and total water-column suspended material content in the case of shallow water not exceeding 20 m depth.

Appendix B of this report describes the use of satellite remote sensing data in the modelling of the transport of suspended sediment in the North Sea. It focuses on NOAA/AVHRR data and describes the various aspects of data processing and corrections as being routinely applied by KNMI. Afetr an overview of available processed data for use PROMISE, the basic procedure of the data-assimilation of these data, designed by Vos and Schuttelaar (1995), is described. The latter concept forms the starting point for the sediment modelling in PROMISE as envisaged by Delft Hydraulics.

## 2.8 Sea ice

Sea ice is not generally an operational problem in the North Sea area, except perhaps locally in some coastal regions of Scandinavia and under severe winter conditions on the German and Dutch coasts. A brief overview of remote sensing capabilities for operational sea ice detection is given in section 3.5 of Johannessen et al. (1996b).

# 3 Sensors for which remote sensing data are or will be available

## 3.1 Introduction

This section covers the satellite-based sensors which provide, or which will provide within the next five years, data which will be relevant to the activities addressed, broadly, by PROMISE.

Table 3 gives an overview of current and near-future satellites important for improving oceanographic forecasts and monitoring. The parameters listed here are sea surface temperature, surface waves, wind, surface ocean features, and seawater composition, each related to a spatial scale.

For the purposes of the PROMISE project, we are interested in obtaining data for the following periods and locations:

(a) North Sea, 49°N–65°N, 6°W–13°E: May 1986—March 1987, January 1988—December 1989, March 1994—September 1994, October 1994—February 1996.

(b) Bay of Biscay, 41°N—50°N, 18°W–0°W: October 1994—present.

## 3.2 Optical and near-infrared sensors

Remote sensing of ocean colour has proved to be of invaluable help in mapping and monitoring the marine environment and its biogeochemical and physical processes, providing information on a score of key parameters for the assessment of physical and ecological mechanisms in coastal region.

Multispectral imagery in the visible part of the spectrum is acquired routinely by satellites (at present e.g. NOAA-AVHRR, Landsat, SPOT, IRS, ADEOS[2] ) as well as from aircraft in dedicated flights. Current as well as planned satellite missions achieve high spectral resolution or very high spatial resolution:

- Although the SeaWiFS programme has been seriously delayed and the satellite on which it is to be carried (SeaSTAR) is now planned to be launched on July 18th 1997, the situation as regards ongoing and future observations has now improved, as a result of the launch of the Indian IRS-P3 satellite in March 1996, the Russian PRIRODA satellite (MIR platform) in April 1996, and the Japanese Advanced Earth Observing Satellite (ADEOS) August 1996. The first two of these satellites carry the Modular Optoelectronic Scanner developed by the DLR Institute of Space Sensor Technology in Germany, and the ADEOS satellite carries the Ocean Color and Temperature Scanner (OCTS) developed by the National Space Development Agency of Japan[3]. Unfortunately, at the present date, there does not appear to be easy access to the

---

[2] ADEOS data transmission has ceased permanently

[3] ADEOS/OCTS data transmission has ceased permanently

Table 3: An overview of current (1997), and near-future (italics), satellites/sensors important for improving oceanographic forecasts and monitoring. Proposed launch dates are in parentheses.

| Scale (size of image) | Sea surface temp. | Waves | Wind | Ocean features (current patterns & slicks) | Sediments Phot. Pigments Biomass |
|---|---|---|---|---|---|
| Global | METEOSAT GOES | | | METEOSAT GOES | |
| Regional | DMSP (SSM/I) | ERS 2 (SAR/ altim./scatt.) | DMSP (SSM/I) | NOAA/AVHRR | |
| (5000 km) | NOAA/AVHRR | JERS 1 (SAR) | ERS 2 (scatt., altim.) | | |
| | ERS-ATSR | GEOSAT(altim.) | JERS 1 (SAR) | JERS-1 (SAR) | SeaSTAR (SeaWiFS) ('97) |
| | Envisat (MERIS) ('99) | RADARSAT (SAR) Envisat ('99) (alt/SAR) | RADARSAT (SAR) Envisat (alt/SAR) | SeaSTAR ('97) (SeaWiFS) Envisat ('99) (SAR) | Envisat ('99) (MERIS) |
| Meso (100–500 km) | NOAA/AVHRR | ERS 2 (alt./SAR) JERS1 (SAR) | ERS 2 (SAR/alt/ /scatt.) JERS 1 (SAR) | NOAA/AVHRR ERS 2 (SAR) | LANDSAT SPOT |
| | ERS-ATSR Envisat MERIS ('99) | RADARSAT (SAR) Envisat SAR ('99) | RADARSAT (SAR) Envisat (SAR) ('99) | LANDSAT SPOT JERS 1 SeaSTAR (SeaWiFS)('97) Envisat ('99) QuickBird ('97) EarlyBird ('98) Orbview('98) | NOAA/AVHRR IRS/MOS Envisat MERIS ('99) SIS ('97) QuickBird |
| Local (~ 1 km) | Aircrafti | Aircraft | Aircraft | Aircraft SPOT | Aircraft SPOT QuickBird ('97) SIS ('97) |

MOS data, from either the Russian or the Indian satellite, and the OCTS data are no longer available.

Future data are likely to be available from the American SEAWiFS instruments which finally will be launched in summer 1997 and MODIS (MOderate Resolution Imaging Spectroradiometer (1998), and from the European MERIS (MEdium Resolution Imaging Spectrometer) onboard ENVISAT platform (1999).

- QuickBird, EarlyBird, SIS, CTA and ORBVIEW are all planned to carry very high-resolution (1–3 m resolution) sensors. They are all scheduled for launch before 1999, starting spring 1997 with EarlyBird).

To obtain simultaneously high spatial and spectral resolution as needed for monitoring of coastal water composition, aircraft equipped with spectrometers such as CASI or DAIS-7915 (DLR, Germany) are the only option available at present. However, the emergence of new concept and processing tools for the fusion of multi-resolution remote sensing data open new fields of investigation to improve that purpose (Mangolini et al., 1994; Ranchin, 1994; Wald et al., 1997).

Dedicated satellite measurements of ocean colour for the periods relevant to the PROMISE modelling effort are sparse, as the Coastal Zone Color Scanner (CZCS) was at the end of its life and not functioning reliably by May 1986. The lack of dedicated ocean colour Earth observation sensors during the last decade means that there are high expectations for the performance of this type of sensor planned for launch by all major space agencies during the next 3 years (Pettersson and Skrøvseth, 1992). In order to be able to discriminate the various ocean constituents contributing to the surface spectral signal, these new sensors will have better optimised and additional spectral channels, compared with CZCS.

## Phytoplankton distribution and primary production

Algorithms are available that convert the optical signal to give a chlorophyll concentration that is representative of the upper attenuation length (Platt et al., 1988). The most commonly used algorithms employ ratios of reflectances at two wavelengths. If we denote reflectance by $R$, these algorithms are of the form $C_s = A_1(R_{\lambda 1}/R_{\lambda 2})^{A_2}$., where $C_s$ is the satellite-weighted pigment concentration and $A_1$ and $A_2$ are constants determined empirically. For the CZCS, the wavelength pairs used are 440 and 550 nm (for $C_s < 1.5\text{mg.m}^{-3}$), and 520 and 550 nm (for $C_s > 1.5\text{mg.m}^{-3}$).

With these algorithms, maps can be produced that show the field of satellite-weighted chlorophyll concentration at regional scale. Such maps have already given useful insights into the ecological dynamics of the pelagic zone.

The description of the methods used to retrieve primary production from the photosynthetic-pigment maps is outside the scope of this report. Recent advances in that field may be found in Platt and Sathyendranath (1991 1993).

## Coloured dissolved organic matter (CDOM)

The near-shore waters undergo flooding of terrigeneous organic material, commonly referred to as yellow substances or gelbstoff. These substances can have a significant impact on the total upwelling radiance signal leaving the water. Because of their landside origin, they are important indicators of water quality (Ferrari and Tassan, 1992; Doerffer, 1990; Tassan, 1988; Maritorena and Guillocheau, 1996). The European MERIS hahas been designed to give a high capability to retrieve CDOM by integrating specific spectral bands.

## Retrieving coastal sediment loads from imagery in visual bands

Suspended inorganic particles (SS) present typical scattering properties that modify the light field distribution into the water column and thus influence the water-leaving radiances measured by remote sensors. Marine radiances can be retrieved from measurements of ocean colour by spectrometers and radiometers. The 0.6 to 0.8 $\mu$m wave band is best sensitive to suspended sediment concentration, as shown by Tassan and Sturm (1986), Curran and Novo (1988), Xia (1993), and Vos and Schuttelaar (1995).

SPOT and LANDSAT data have been used to detect sediments. In the future new instruments with spectral bands specified by optimal sediment retrieval will be available. This will be the case of the European MERIS on ENVISAT (Doerffer et al., 1995). Coupled with great improvement in atmospheric correction capabilities, it could be one of the main tool for sediment transport monitoring.

In PROMISE, analyses of CASI data of the Holderness coast are made based on survey data collected by the Environmental Agency in the UK within a program to carry out routine aircraft surveys of British coastal waters. The imagery is acquired in 15 narrow spectral bands, ranging in wavelength from 400 to 800 nm.

In order to derive the spatial distribution of the sediment load in coastal waters, these data have to undergo several processing steps.The two first steps are common to any satellite optical data processing in order to derive biogeo-physical quantities from an electromagnetic signal measured by a remote sensor. However the corrections to be applied are highly dependent upon the sensor and air/space-craft used: :

- the digital counts of the spectrometer have to be translated to radiances using system calibration data;

- atmospheric influences (contribution of path radiance, attenuation of the signal) have to corrected for to obtain the surface reflectance, and surface effects need to be corrected for to obtain subsurface reflectance. This step is often done in relation with geometric correction since radiometric distorsion also occur because of geometric distorsion;

- given the spectral behaviour of the absorption and backscatter of the different constituents present in the water, the concentrations of these constituents have to be derived from the subsurface reflectance data.

- Observed patterns in the sediment load need to be interpreted to obtain useful information, by linking these data to the seabed topography and composition and the current and wave conditions. In PROMISE, the focus is on the use of sediment transport models, and the assimilation of the remote sensing data into these models.

The atmospheric contribution to the signal is calculated with the model MODTRAN (Anderson et al., 1994). With this model, the observed radiance is separated in path radiances due to the scattering of light by molecules and aerosols, and in a water-leaving radiance. Taking into account the amount of sunlight reaching the water surface, this results in a surface reflectance ratio $R$ for each of the 15 spectral bands available from the CASI. Critical aspects are the sensitivities to unknown or spatially variable atmospheric constituent concentrations and the assumptions needed to be able to extract information from the image itself to calibrate the aerosol contribution.

It is commonly assumed that the subsurface reflectance depends only on inherent properties of the water column, and not on the instantaneous light climate. Gordon et al. (1975b) proposed that the subsurface reflectance ratio depends in the following way on the total absorption coefficient $a$ and backscattering coefficient $b_b$ of the water and its suspended constituents:

$$R = F \left( \frac{b_b}{a + b_b} \right) ,$$

where $F$ is an arbitrary function, usually a first or second order polynomial. The total absorption and backscattering coefficients are the sums of the individual coefficients of the different absorbers and scatterers which are present (Preisendorfer, 1961) Given the spectral dependence of the absorption and scattering coefficients of the water and its suspended contents, the observed values of the subsurface reflectance can be used to retrieve the concentrations of these constituents. Pure water absorbs the longer wavelengths within the visual spectrum and scatters the shorter wavelengths, and hence appears as blue. The effect of chlorophyll on the water colour varies with age and species, but in general it absorbs blue light. The effect of inorganic suspended matter, such as sand and silt, is also variable. In general the reflectance increases for all wavelengths with increasing load, leaving the water colour unchanged. The situation may be different in cases where the sediment is highly coloured.

## Bathymetry and bottom mapping

Because remote sensing only deals with the surface or upper layer of the oceans, information on bathymetry from visual and infra-red observations can only be obtained in shallow water where measurements of light beam attenuation by radiometer or spectrometer can be used to derive the depth (Lyzenga, 1978; Bierwirth et al., 1993; Maritorena et al., 1994).

The usefulness of such techniques for mapping water body bottoms has been demonstrated by several authors in various media, e.g. inland-water, shallow coastal zone waters. The best results were obtained for the mapping of coral reefs and barriers (Fagoonee, 1986;

Maritorena et al., 1994). However, significant results have been observed for more turbid areas Tassan and d'Alcala (1993).

## 3.3 Thermal infrared

*AVHRR data for computing SST* Sea surface temperature (cloud-limited data) can be computed from NOAA AVHRR thermal IR channels ($\approx$10.5–12.5 $\mu$m), with a resolution of 1 km and a swath width of 2000 km. Data exist at Eurimage since the early 1980s. Daily wide-swath data are available from Eurimage (via Tromsø Satellite Station). If cloud conditions are unknown, visual quick-look should be ordered before the cloudfree scenes are selected. Routines for processing of satellite-calibrated SST from raw data exist at NERSC.

*SST computed from ATSR data* SST is available from ERS ATSR processed data (cloud limited), with a. resolution of 1 km and a swath width of 500 km. Data exists at ESA since the autumn of 1991 and should be available from ESA.

## 3.4 Passive microwave

*SSMI Brightness data for computing wind speed* Wind is computed from measurements of brightness temperatures (emissivity) by the DMSP SSMI passive microwave instrument, with a resolution of 50 km and a swath width of 1400 km (Fung, 1994; Skofronick-Jackson and Gasiewski, 1995; Dickinson and Brown, 1996). NERSC has CD-ROMs with brightness temperature data from autumn 1987. Routines for determining wind speed (not direction) are available, but are not at present held or tested at NERSC. The wind-speed retrieval is stability-dependent (Pospelov, 1996), and the presence of atmospheric moisture makes the process more difficult.

It is possible to measure temperature and salinity from passive microwave observations. Accuracies of ±1 deg C and ±1 part per thousand (ppt) in salinity and are achievable Blume and Kendal (1982), but since relatively long wavelengths are involved, the resolution is too poor with satellite sensors for coastal seas such as the North Sea, and it would be necessary to use airborne instruments.

## 3.5 Radar

### 3.5.1 Radar altimeter

Satellite radar altimeters can determine the significant wave height by the slope of the returned pulse. The wind speed can be determined, using empirically-derived algorithms, from the backscattering cross-section ($\sigma^0$).

The GEOSAT altimeter operated from March 1985 to January 1990 (Wu et al., 1994). The wind speed accuracy specification was ±1.8 m s$^{-1}$ over the range 1–18 m s$^{-1}$ (MacArthur et al., 1987; Dobson and Chaykovsky, 1990). Contamination of the radar return by

reflections from land may occur: Challenor et al. (1990) assumed that the signal was unreliable up to $\approx$ 42 km from the shoreline, and Wu et al. (1994) detected apparent land contamination at greater distances.

The altimeters on SEASAT and the ERS-1/2 satellites have similar performances, and in general it can be said that for wind speeds are accurate to $\pm 2\,\mathrm{m\,s^{-1}}$ for moderate winds $(3\text{–}12\,\mathrm{m\,s^{-1}})$, with decrasing accuracy at higher wind speeds, the instruments becoming unreliable above $25\,\mathrm{m\,s^{-1}}$(Romeiser, 1993; Komen et al., 1994). Wave height accuracies are about 10% for the range 1–20 m, although some investigations have reported that the altimeter underestimates wave heights of 4 m and above when compared with buoy data (Goodberlet et al., 1992; Günther et al., 1993; Komen et al., 1994).

*TOPEX/POSEIDON*: The TOPEX/POSEIDON radar altimeter can be used for computing significant wave height and wind speed. A data set for the relevant periods has been converted to ASCII and is available from NERSC. ERS altimeter data are also suitable for this purpose.

### 3.5.2 ERS scatterometer data for computing wind velocity

Wind is computed from measurements of surface roughness by ERS scatterometer radar, resolution 50 km, swath width 500 km. (See section 2.4.) Tapes with $\sigma^0$ (raw data) exist at NERSC since the autumn of 1991. The ERS scatterometer winds have been assimilated routinely in the atmospheric circulation models of The Norwegian Meteorological Institute (DNMI) since 1995 (Breivid and Haugse, 1994; Breivid et al., 1995).

### 3.5.3 Imaging radars

In addition to synthetic aperture radar, there are satellite-based real-aperture radars deployed. In particular, the Russian (Okean series) and Ukrainian (Sich) side-looking radars (SLR) have $\approx$ 2 km resolution over a swath width of about 450 km. They are mainly used for sea-ice monitoring, but they do show the wind speed. Their absolute calibration is, however, not so stable as that of the ERS satellites.

### Synthetic aperture radar (SAR)

Synthetic aperture radar data are available from ERS-1/2 (since 1991) JERS-1 and RADARSAT (since 1995). The ERS data are available in 100 km swaths at a typical resolution of 30 m. The data can be used to obtain qualitative information on current patterns and surface slicks: quantitative information is available for wind variations on scales of $\sim$ 1 km, and on surface waves (direction and wavelength, and a rough indication of wave amplitude, for waves of wavelength longer than about 60 m). For the PROMISE areas, this generally means that waves are resolved frequently only over the Bay of Biscay location, which is well exposed to swell from the North Atlantic. It can be useful to use SAR in the Bay of Biscay area to provide some input and validation data for the wave modelling activity in PROMISE.

Routine monitoring using SAR is difficult at present, since images are available at best at intervals of the order of 3–6 days. This can be improved somewhat by making use of the 500 km swath of the ScanSAR mode of RADARSAT, with the disadvantage of poorer resolution (say 150 m) and greater expense (USD 4000 per image).

## SAR data coverage and availability

A large number of SAR images were acquired during the operational phases of ERS-1 (1991 to 1996) and its successor ERS-2 (from 1996). The majority of the stored SAR images cover areas in the northern hemisphere, and available images can be looked for using a database search tool developed by ESA. Search keys may be geographical location, time frame or more specific parameters as orbit number or frame number. A combination of the search keys is, of course, possible, to derive the ordering specifications for a preferred SAR image. Lists for planned short term future SAR image acquirements are also available on request. The data acquisition is very often directed by ongoing campaigns or user requirements for specific scientific or technical purposes.

The recently-launched (1995) Canadian satellite RADARSAT was designed primarily for ice monitoring purposes, having HH rather than VV polarization of the transmitted/received radar signal. However, it is nevertheless capable of monitoring open ocean phenomena, and it is possible to use it in a number of different incidence angle and resolution modes. The widest swath width available is 500 km, and it is also possible to obtain high-resolution images at a wide range of incidence angles, so that there is a good potential for more frequent coverage of specific locations.

*Wave spectra computed from ERS-SAR-Wavemode*: Wave-mode SAR wave spectra are obtained for $\approx 5 \times 5$ km imagettes every 200–300 km along the orbit. Data processed to wave spectra can be obtained from ESA archives, since the autumn of 1991. It is necessary to use an inversion algorithm, combined with a good 'first guess' from e.g. a wave model.

Image mode SAR data may also be used for generating wave spectra. Approximately 40 full-resolution ERS-1/2 SAR images have been obtained by NERSC/POL/Clima Marítimo specifically for PROMISE. There is a possibility that the 180° directional ambiguity in SAR wave spectra may be resolved by processing complex SAR data (Engen and Johnsen, 1995).

Noticeable features of SAR images include bright and dark linear structures, often wound into wavelike or spiral patterns, which are associated with regions where there are spatial gradients of the current. These are a result of wave-current interaction enhancing (or diminishing) the surface roughness, principally at or near the Bragg scattering wavelength $2\lambda_R \sin\theta$, where $\lambda_R$ is the radar wavelength and $\theta$ is the incidence angle. It is, however, not easy to quantify the actual values of the currents involved which generate such features, though some progress has been made in specific areas such as the monitoring of shallow-water bathymetry and of internal waves.

## Overview of the satellite image database system at NERSC

At present, the ERS SAR image database at NERSC contains a description of and a quick-look for nearly 4000 scenes. Most of these images are located in Arctic areas, but the database also contains a number of images from the North Sea, and some from the North Atlantic, the Spanish coast, the Gulf of Finland, the St. Petersburg area and the Antarctic.

For each SAR scene a description of its location, acquisition time, sensor and satellite parameters, wind measurements (if available from other sources), and any number of keywords is kept. A quick-look is also stored for each scene. This is a resampled and compressed version in JPEG format that contains the major features of the original image.

Examples of phenomena that can be seen in the quick-look include, atmospheric and oceanic fronts, sea ice features, ship tracks in ice and open ocean, internal waves, eddies, vortex pairs, wind sheltering, natural film and oil spills.

Queries can be made by specifying geographic area, time range of interest, a wind speed interval and keywords. A list of all images satisfying the given search criteria is then presented (Fig. 10), and the user can select any of these for further inspection (of metadata) or for display of quick-looks (Fig. 11). Even though the size of a quick-look is typically about 5% of the size of the original image, the quality is sufficient for browsing and in many cases enables the user to decide whether the images are suitable for a specific study. Maps showing the coverage of the selected SAR scenes can also be generated (Fig. 12). This is particularly useful when looking for overlapping images in a particular area and season. These maps can also be annotated with image date or orbit+frame number within the respective rectangle.

The image database archive is implemented on a Silicon Graphics Crimson computer, under Unix System V. The Oracle RDBMS (Relational DataBase Management System), version 7.1, is used to manage the data. Oracle Forms, version 3.0, is used to build the user interface, and data manipulation is done by means of embedded SQL and C programs. The database files currently occupy about 175 megabytes, and an additional disk space of about 230 megabytes is needed for the RDBMS and in-house developed software.

Fig. 10: A screen with a list of images satisfying the given search criteria.

## SAR data available specifically for PROMISE

The following SAR data were obtained specifically for the PROMISE project:

```
===================================================================================================
SAR DATA OBTAINED UNDER TANDEM ANNOUNCEMENT OF OPPORTUNITY FOR ERS-1/2

Data from Holderness area (PRI files on Exabyte tape, c.8000x8000 12.5m pixels:

Sat. orbit track frame date time Corner points (deg & min: + = N/E, - = S/W) NERSC file ref
                        UTC                                                    (200m resol. image)
                                                                     /users/fram4/tmpdir/SAR/alastair/


ERS1 22126 094 2511 951008 1100 53d52 -1d09 54d45 -0d49 54d33 +0d40 53d40 +0d18 S081095_1.ps
ERS1 22126 094 2529 951008 1101 52d59 -1d28 53d52 -1d09 53d40 +0d18 52d47 -0d02 S081095_2.ps
ERS2 02453 094 2529 951009 1101 52d59 -1d28 53d52 -1d09 53d40 +0d18 52d47 -0d02 S091095_1.ps
ERS2 02453 094 2511 951009 1100 53d52 -1d09 54d45 -0d49 54d33 +0d40 53d40 +0d18 S091095_2.ps

ERS1 22355 323 2511 951024 1058 53d52 -0d26 54d45 -0d05 54d33 +1d23 53d40 +1d01 S241095_1.ps
ERS1 22355 323 2529 951024 1058 52d59 -0d45 53d52 -0d26 53d40 +1d01 52d47 +0d40 S241095_2.ps
ERS2 02682 323 2511 951025 1058 53d52 -0d26 54d45 -0d05 54d33 +1d23 53d40 +1d01 S251095_1.ps
ERS2 02682 323 2529 951025 1058 52d59 -0d45 53d52 -0d26 53d40 +1d01 52d47 +0d40 S251095_2.ps

ERS1 22856 323 2529 951128 1058 52d59 -0d45 53d52 -0d26 53d40 +1d01 52d47 +0d40 S281195_1.ps
ERS2 03183 323 2529 951129 1058 52d59 -0d45 53d52 -0d26 53d40 +1d01 52d47 +0d40 S291195_1.ps

ERS1 23357 323 2529 960102 CANCELLED - POOR DATA QUALITY (ESA/ESRIN - Sara Violetti 1996sept16)
ERS1 23357 323 2511 960102 1057 53d52 -0d26 54d45 -0d05 54d33 +1d23 53d40 +1d01 S020196_1.ps
ERS2 03684 323 2529 960103 1058 52d59 -0d45 53d52 -0d26 53d40 +1d01 52d47 +0d40 S030196_2.imf
ERS2 03684 323 2511 960103 1058 53d52 -0d26 54d45 -0d05 54d33 +1d23 53d40 +1d01 S030196_1.imf


Data from Bay of Biscay (PRI files on Exabyte tape, c.8000x8000 12.5m pixels:
```
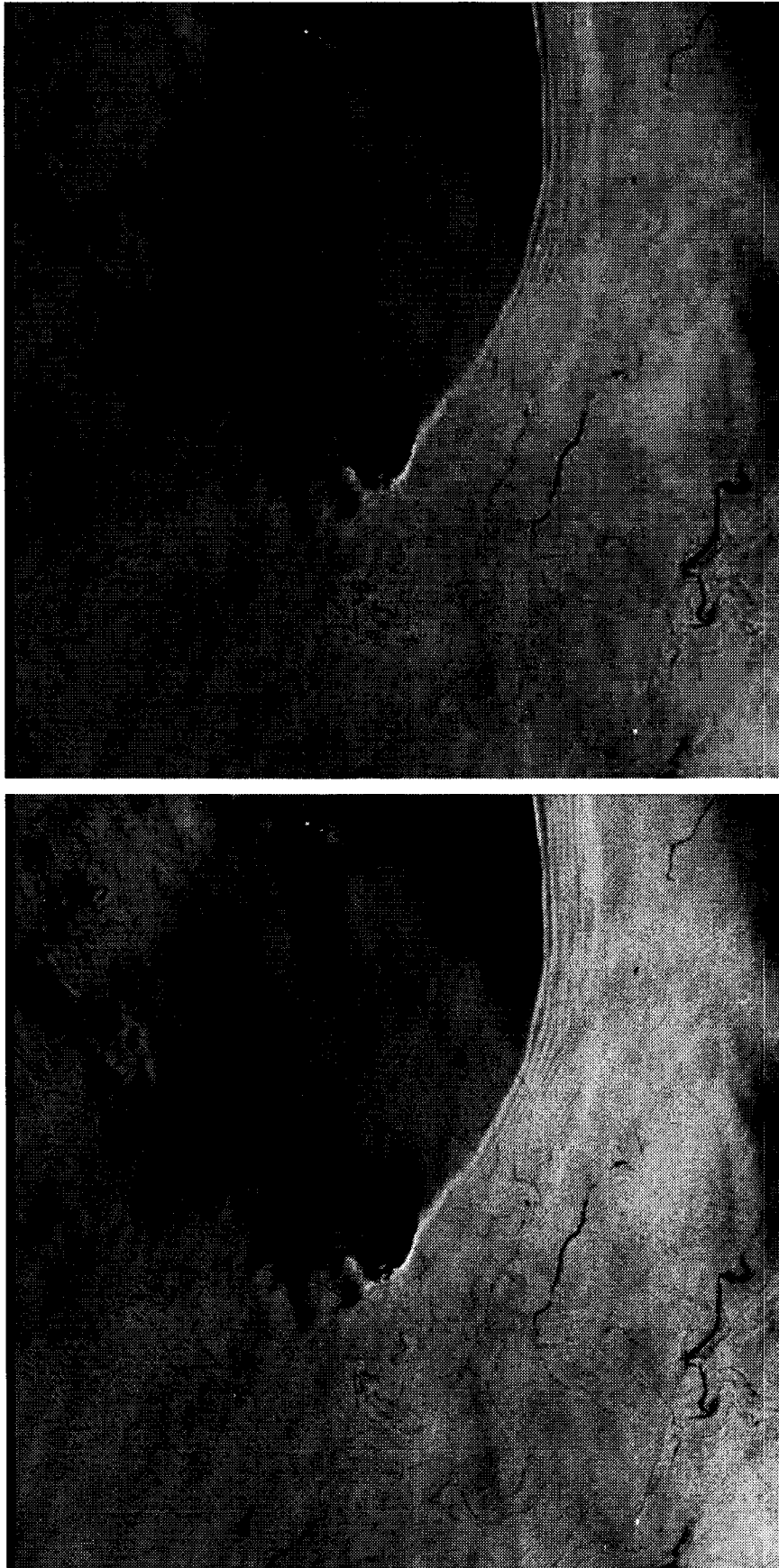
Original Data © ESA/TSS 1996. Image Processing NERSC

Fig. 11: Example of quick-look from the NERSC archive and the original image.
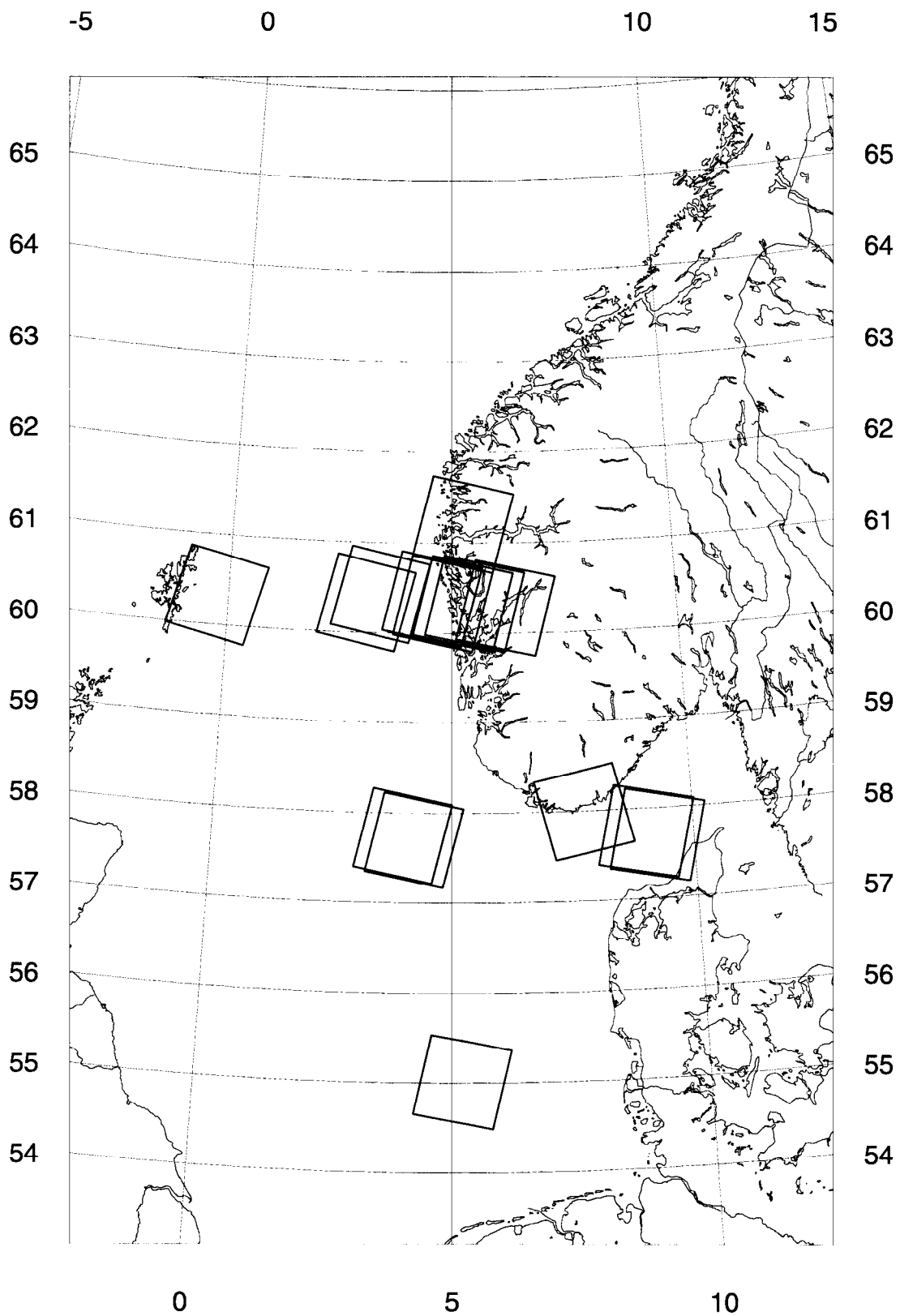
Fig. 12: Example of SAR coverage map generated by the NERSC image archive system.

42

```
Sat. orbit track frame date time Corner points (deg & min: + = N/E, - = S/W) NERSC file ref
                       UTC                                              (200m resol. image)
Ascending orbits:


ERS1 23135 101 0855 951217 2221 43d20 -2d51 43d31 -1d40 42d37 -1d25 42d26 -2d35 S171295_1.imf
ERS1 23135 101 0873 951217 2221 44d13 -3d08 44d24 -1d55 43d31 -1d40 43d20 -2d51 S171295_2.imf


ERS2 03462 101 0855 951218 2221 43d20 -2d51 43d31 -1d40 42d37 -1d25 42d26 -2d35 S181295_1.imf
ERS2 03462 101 0873 951218 2221 44d13 -3d08 44d24 -1d55 43d31 -1d40 43d20 -2d51 S181295_2.imf


ERS1 24638 101 0855 960331 2221 43d20 -2d51 43d31 -1d40 42d37 -1d25 42d26 -2d35 S310396_1.imf
ERS1 24638 101 0873 960331 2221 44d13 -3d08 44d24 -1d55 43d31 -1d40 43d20 -2d51 S310396_2.imf


ERS2 04965 101 0855 960401 2221 43d20 -2d51 43d31 -1d40 42d37 -1d25 42d26 -2d35 S010496_1.imf
ERS2 04965 101 0873 960401 2221 44d13 -3d08 44d24 -1d55 43d31 -1d40 43d20 -2d51 S010496_2.imf


Descending orbits:


ERS1 21854 323 2691 950919 1059 45d01 -3d20 45d55 -3d04 45d43 -1d50 44d50 -2d07 S190995_1.imf
ERS1 21854 323 2709 950919 1100 44d08 -3d36 45d01 -3d20 44d50 -2d07 43d57 -2d23 S190995_2.imf
ERS1 21854 323 2727 950919 1100 43d15 -3d51 44d08 -3d36 43d57 -2d23 43d04 -2d39 S190995_3.imf


ERS2 02181 323 2691 950920 1059 45d01 -3d20 45d55 -3d04 45d43 -1d50 44d50 -2d07 S200995_1.imf
ERS2 02181 323 2709 950920 1100 44d08 -3d36 45d01 -3d20 44d50 -2d07 43d57 -2d23 S200995_2.imf
ERS2 02181 323 2727 950920 1100 43d15 -3d51 44d08 -3d36 43d57 -2d23 43d04 -2d39 S200995_3.imf


ERS1 22312 280 2709 951021 1054 44d08 -2d09 45d01 -1d54 44d50 -0d40 43d57 -0d57 S211095_1.imf
ERS1 22312 280 2727 951021 1054 43d15 -2d24 44d08 -2d09 43d57 -0d57 43d04 -1d13 S211095_2.imf


ERS2 02639 280 2709 951022 1054 44d08 -2d09 45d01 -1d54 44d50 -0d40 43d57 -0d57 S221095_1.imf
ERS2 02639 280 2727 951022 1054 43d15 -2d24 44d08 -2d09 43d57 -0d57 43d04 -1d13 S221095_2.imf


ERS1 22355 323 2691 951024 1059 45d01 -3d20 45d55 -3d04 45d43 -1d50 44d50 -2d07 S241095_1.imf
ERS1 22355 323 2709 951024 1100 44d08 -3d36 45d01 -3d20 44d50 -2d07 43d57 -2d23 S241095_2.imf
ERS1 22355 323 2727 951024 1100 43d15 -3d51 44d08 -3d36 43d57 -2d23 43d04 -2d39 S241095_3.imf


ERS2 02682 323 2691 951025 1059 45d01 -3d20 45d55 -3d04 45d43 -1d50 44d50 -2d07 S251095_1.imf
ERS2 02682 323 2709 951025 1100 44d08 -3d36 45d01 -3d20 44d50 -2d07 43d57 -2d23 S251095_2.imf
ERS2 02682 323 2727 951025 1100 43d15 -3d51 44d08 -3d36 43d57 -2d23 43d04 -2d39 S251095_3.imf


ERS1 25089 051 2691 960502 1056 45d01 -2d37 45d55 -2d21 45d43 -1d07 44d50 -1d23 S020596_1.imf
ERS1 25089 051 2709 960502 1057 44d08 -2d52 45d01 -2d37 44d50 -1d23 43d57 -1d40 S020596_2.imf
ERS1 25089 051 2727 960502 1057 43d15 -3d08 44d08 -2d52 43d57 -1d40 43d04 -1d56 S020596_3.imf


ERS2 05416 051 2691 960503 1056 45d01 -2d37 45d55 -2d21 45d43 -1d07 44d50 -1d23 S030596_1.imf
ERS2 05416 051 2709 960503 1057 44d08 -2d52 45d01 -2d37 44d50 -1d23 43d57 -1d40 S030596_2.imf
ERS2 05416 051 2727 960503 1057 43d15 -3d08 44d08 -2d52 43d57 -1d40 43d04 -1d56 S030596_3.imf


================================================================================================
SAR DATA OBTAINED FROM DRA, WEST FREUGH, IN COLLABORATION WITH PROUDMAN OCEANOGRAPHIC
LABORATORY AND CLIMA MARITIMO

Data is 8000x8768 12.5m pixels, single look complex format, resolution 28 x 24 m

Holderness area:

Satellite Orbit pass date  time centre pos.   Exabyte tape ref.
ERS1      22627 094 951112 1100 54.24N 00.26W  WFE8971
ERS1      22856 323 951128 1058 54.24N 00.48E  WFE8972
```

```
ERS1      23128 094 951217 1100 54.64N 00.09W   WFE8973

Bay of Biscay:

ERS1      20852 323 950711 1100 43.92N 03.03W   WFE8970
ERS1      21081 051 950727 1058 43.86N 02.34W   WFE8969
ERS1      21582 051 950831 1058 43.86N 02.33W   WFE8968
ERS2       1909 051 950901 1058 43.86N 02.33W   WFE8530
ERS2       2138 280 950917 1055 43.87N 01.61W   WFE8964
ERS1      22083 051 951005 1058 43.87N 02.34W   WFE8966
ERS2       3684 323 960103 1100 43.93N 03.04W   WFE8965

=====================================================================================
```

The above high-resolution image-mode data should be usable for verifying model input (wind forcing), and wave-model output (specifically dominant wavelength and period for areas exposed to the open ocean).

### 3.5.4 Land-based, marine and platform-based radar

A number of radar systems are available which can monitor oceanographic processes from surface locations. These include attachments to land-based or ship-borne marine radar equipment which can measure surface waves, at least the dominant wavelength and direction, and which may be able to detect sufficiently strong currents by their effect on the wave propagation velocity. There are also more sophisticated platform-based radars (e.g. one produced by the company 'MIROS') which can measure wave orbital velocities directly and thus provide quantitative information on wave height and wave spectra, as well as determining the local current velocity.

### 3.5.5 HF radar

If long-wavelength electromagnetic waves are used (wavelengths of several metres or more), one has direct Bragg scattering from wind-wave components. Such 'HF' radars are generally shore-based, and can measure Doppler shifts due to radial currents, as well as the movements of other strong reflectors such as ships (see p. 6). Systems available commercially include 'CODAR' and 'OSCR'.

# 4 Suitability of data for operational requirements

## 4.1 Data coverage

There is generally a trade-off between the spatial resolution of satellite data and its available temporal coverage. Continuous, nearly global coverage is afforded by geostationary meteorological satellites, and coverage several times daily is available for NOAA AVHRR. These optical and infra-red data are only available under cloud-free conditions, which is a significant disadvantage for mid-latitude locations which are subject to frequent poor weather.

Passive microwave and radar sensors can penetrate cloud cover, but the former sensors generally have rather too poor resolution for covering North Sea scales. The detail available in SAR images is good, but the coverage is only every few days at present, though there is a possibility of improvement in data coverage with the use of the recently launched RADARSAT.

## 4.2 Availability in near-real time

Availability of satellite data in near-real time is now quite good, certainly as regards such sensors as NOAA AVHRR and ERS SAR. However, the real-time capability of AVHRR and other optical/infrared sensors for the end user is substantially degraded by their only being available under cloud-free conditions.

It is possible to make arrangements with such organizations as Tromsø Satellite Station (in Norway), KNMI (in The Netherlands) and RAIDS (in the U.K.) to read and process satellite data, and send it to an onshore analysis facility (such as NERSC, KNMI, or Argoss), who can then produce an interpreted satellite data chart which can in turn be sent out to end users such as vessels operating in the relevant area. KNMI has a large experience with the processing of NOAA/AVHRR data and its distribution to end users (see Appendix B).

The time taken for this whole procedure can be 90 minutes or less. Satellite image data can also be transmitted from shore to ship via INMARSAT.

For specific types of data (e.g. altimeter and SAR Wave Mode), the data are processed on a routine basis and distributed via the Global Telecommunications System to national meteorological centres, for use in their meteorological analysis, modelling and forecasting services.

## 4.3 Programme continuity and long term data access

Operational issues require the certainty to get access to the useful data over years. This can be achieve by several ways:

- by considering series of a given sensors, e.g. SPOT, NOAA or Landsat series,

- by assuring a good enough similitude in data acquired by different sensors in order to enable to use them indifferently within a given model, e.g. ERS-SAR and RadarSat SAR,

- by setting up transform rules to simulate a particular sensor data from another sensor measurements,

- by implementing models using different inputs but which assure the comparability of the derived parameters. This approch will be used to take advantage of the various "ocean colour" sensors that will be available in the next three years

## 4.4 Data assimilation

When interpreting remote sensing data it is important to consider that satellites only observe the Earth's surface. In order to achieve three-dimensional marine information and forecasts, remote sensing data together with in-situ data must be assimilated in numerical models.

There has, over the last decade, been a rapid development of various data assimilation methods which can be used with ocean hydrodynamic and ecosystem models. At present, however, none of these methods are used operationally, at least partly because the necessary observational data are either insufficiently accurate or do not provide sufficiently good coverage.

In a fully operational system the access time for the most recent observations also becomes important. Real time analyses and predictions from the European weather services must be used to ensure a proper forcing of the model and to make it possible to generate realistic predictions of the marine system.

For the simultaneous assimilation of NOAA/AVHRR reflection imagery and *in situ* data in the suspended sediment model, a method based on that described in Vos and Schuttelaar (1995) will be used within PROMISE. For a concise description of this, see Appendix B. A study will also be made on the feasibility of assimilating SAR and/or altimeter data into wave models for the Bay of Biscay location.

Appendix C gives a concise overview of the basic principles, applicability, and experience, and the key issues and challenges in data assimilation as foreseen within the framework of EUROGOOS. This is equally relevant for PROMISE.

## 5 Concluding remarks

This report summarizes the available remote sensing information which may be useful for the hydrodynamic, wave and sediment modelling activities within PROMISE, and also the prospects of obtaining new data within a 3–5 year time horizon. The data currently available which appear to be of greatest practical use are

- NOAA/AVHRR optical and infra-red observations, for the charting of sea-surface temperature variations and the observations of surface sediments Vos and Schuttelaar (1995); Vos et al. (1997).

- Observations of surface waves by satellite altimeter (see Appendix A), and SAR. SAR gives directional information for swell waves, but suffers from poor temporal coverage for any one location.

- Observations of wind by radar scatterometer (50 km resolution), and by SAR (1 km resolution).

For better estimation of suspended sediment, chlorophyll etc., more detailed spectral information in the optical and near-infrared bands were available from the Coastal Zone Color Scanner in the period 1978–1986. Unfortunately, it still appears that the proposed launch of SeaWiFS aboard SeaSTAR in July 1997 provides the best prospect of easy future access to data of such good quality.

By focusing on applied research toward operational services, remote sensing will, in synergy with *in situ* and modelling data, contribute to benefit individual industries and activities as listed in Woods et al. (1996). It is important that relations between the remote sensing and user communities are further developed and that focus is set on future user needs.

# References

Aksnes, D. L., Aure, J., Furnes, G. K., Skjoldal, H. R., & Sætre, R. (1989) Analysis of the *chrysochromulina polylepis* bloom in the Skagerrak, May 1988: Environmental conditions and possible causes. Technical Report 89/1, IBM Bergen Scientific Centre, Bergen, Norway.

Althuis, I., Vogelzang, J., Wermand, M., Shimwell, S., Gieskes, W., Warnock, R., Kromkamp, J., Wouts, R. & Zevenboom, W. (1996) On the colour of case 2 waters particulate matter. part ii: Instruments. methods and database. Technical report 95-21B, Netherlands Remote Sensing Board, Delft.

Andersen, C. & Smith, P. C. (1989) Oceanographic observations on the Scotian shelf during CASP. *Atmosphere–Ocean*, 27(1):130–156.

Anderson, G. P., Wang, J., Hoke, M. L., Kneizys, F. X., Chetwynd, J. H., Rothman, L. S., Kimball, L. M., McClatchey, R. A., Shettle, E. P., Cluogh, S. A., Gallery, W. O., Abreu, L. W. & Selby, J. E. A. (1994) History of one family of atmospheric radiative transfer codes. In *Proc. Int. Conf. On Passive Infrared Remote Sensing of Clouds and the Atmosphere II, 26–28 Sept. 1994, Rome, SPIE 2309*, pages 170–183.

Bauer, E., Hasselmann, S., Hasselmann, K. & Graber, H. C. (1992) Validation and assimilation of Seasat altimeter wave heights using the WAM wave model. *Journal of Geophysical Research*, 97(C8):12 671—12 683.

Bierwirth, N., Lee, T., & Burne, R. (1993) Shallow sea-floor reflectance and water depth derived by unmixing multispectral imagery. *Photogram. Eng. Remote Sensing*, 59(3):331–338.

Bijaoui, J., Jullien, S. & Cauneau, F. (1994) Bathymetry measurement in shallow water areas using airborne spectrometers. In A. A. Balkema, editor, *Proceedings of the $14^{th}$ EARSeL symposium*, pages 311–314, Rotterdam, The Netherlands.

Bijlsma, A. C., van den Boogaard, H. F. P. & de Smet, A. C. (1991) The assimilation of satellite and *in situ* data in a temperature model of the North Sea. Technical Report 91-24, Delft Hydraulics.

Blume, H.-J. & Kendal, B. M. (1982) Passive micro-wave measurements of temperature and salinity in coastal zones. *IEEE Transactions on Geoscience and Remote Sensing*, GE-20(3).

Breivid, L. A. & Haugse, B. (1994) Scatterometer wind retrieval at the Norwegian Meteorological Institute. Technical Report 124, The Norwegian Meteorological Institute.

Breivid, L. A., Haugse, B. & Sunde, J. (1995) Operational use of scatterometer wind information at the Norwegian Meteorological Institute, DNMI Research Report No. 1.

Breivik, L. A., Reistad, M., Schyberg, H. & Sunde, J. (1996) Application of ocean surface wind and wave information from ERS in atmosphere and ocean monitoring and numerical forecast models. In *ESA*, pages 61–64.

Bricaud, A., Morel, A. & André, J.-M. (1987) Spatial/temporal varability of algal biomass and potential productivity in the Mauritanian upwelling zone, as estimated from CZCS data. *Advances in Space Research*, 7.

Calkoen, C., Snoeij, P., van Halsema, D., Vogelzang, J., Oost, W. A., & Jähne., B. (1991) Evaluation of a two-scale model using extensive radar backscatter and wave measurements in a large wind-wave flume. In *Proc. IGARSS 91*, pages 885–888.

Calkoen, C. J. (1996) ERS-1 survey Plaatgat. Technical Report A013, ARGOSS.

Calkoen, C. J. & Wensink, G. J. (1993) Use of ERS-2 SAR to optimize ship-based bathymetric surveys in the Waddenzee. Technical Report h 1985, Delft Hydraulics, Delft.

Carter, D. J. T., Challenor, P. G. & Srokosz, M. A. (1992) An assessment of GEOSAT wave height and wind speed measurements. *Journal of Geophysical Research*, 97(C7):11 383–11 392.

Carter, D. J. T. & Cotton, P. D. (1996) Applications of wave statistics estimated from altimeter data. In *Proc. Second ERS Applications Workshop, London, 6-8 December, 1995, ESA SP-383*, pages 57–60. ESA Publications Division, Noordwijk, The Netherlands.

Challenor, P. G., Foale, S. & Webb, D. J. (1990) Seasonal changes in the global wave climate measured by the GEOSAT altimeter. *International Journal of Remote Sensing*, 11(12):2205–2213.

Chapron, B., Fouhaily, T. E. & Kerbaol, V. (1995) Calibration and validation of ERS wave mode products. IFREMER Document DRO/OS/95-02.

Clima Marítimo, GKSS, K. U. Leuven, MUMM, & POL. (1997) PROMISE wave modelling, North Sea implementation. Technical Report 47, Proudman Oceanographic Laboratory, Birkenhead, U.K.

Crombie, D. D., (1955) Doppler spectrum of sea echo at 13.56 Mc/s. *Nature*, 175:681–682.

Curran, P. & Novo, E. (1988) The relationship between suspended sediment concentration and remotely sensed spectral radiance: a review. *J. Coastal Res.*, 4(3):351–368.

Dickinson, S. & Brown. R. A. (1996) A study of near-surface winds in marine cyclones using multiple satellite sensors. *Journal of Applied Meteorology*, 35(6):769–781.

Dobson, E. B. & Chaykovsky, S. P. (1990) GEOSAT wind and wave measurements during LEWEX. *Applied Physics Laboratory Tech. D.*, 11(3–4):408–413.

Doerffer, R. (1990) How to derive concentrations of chlorophyll, suspended matter and gelbstoff from multispectral radiances of Case II water. In *ICES'90*. ICES.

Doerffer, R., Sørensen, K. & Aiken, J. (1995) Meris: Potential for coastal zone application. In P. Curran & C. Robertson, editors, *RSS95 - 21ˢᵗ Annual Conference of the Remote Sensing Society*, pages 166–175.

Dundas, I., Johannessen, O. M., Berge, G. & Heimdal, B. (1989) Toxic algal bloom in Scandinavian waters, May–June 1988. *Oceanography*, 2(1).

Engen, G. & Johnsen, H. (1995) SAR–ocean wave inversion using image cross spectra. *IEEE Transactions on Geoscience and Remote Sensing*, 33(4):1047–1056.

ESA, editor. (1996) *Proc. Second Intl Workshop on ERS Applications, London, 1995 December 6–8*. ESA Publications Division ESA SP-383, Noordwijk, The Netherlands.

Estep, L. (1994) Bottom influence on the estimation of chlorophyll concentration in water remotely sensed data. *Int. J. Remote Sensing.*, 15(1):205–214.

Estep, L. & Holloway, J. (1992) Estimators of bottom reflectance spectra. *Int. J. Remote Sensing.*, 13(2):393–397.

Fagoonee, I. (1986) Remote sensing techniques for coral reef studies. In *20ᵗʰ Int. Symp. Remote Sensing of Environment*, volume 1, Nairobi, Kenya. ERIM.

Ferrari, G. M. & Tassan, S. (1992) Evaluation of the influence of yellow substance absorption on the remote sensing of water quality in the Gulf of Naples: a case study. *International Journal of Remote Sensing*, 13(12):2177–2189.

Fung, A. K. (1994) *Microwave scattering and emission models and their applications*. The Artech House remote sensing library. Artech House, Boston.

Furnes, G. K. (1994) Discharges of produced water from production platforms in the North Sea. Technical Report R-064641, Norsk Hydro, Bergen, Norway.

Georges, T. M., Harlan, J. A. & Lematta, R. A. (1996) Large-scale mapping of ocean surface currents with dual over-the-horizon radars. *Nature*, 379:434–436.

Goodberlet, M. A., Swift, C. T. & Wilkerson, J. C. (1992) Validation of the ocean surface wind fields and wave height measurements derived from data of the ERS-1 scatterometer and radar altimeter (early results). In *Proc. Workshop on ERS-1 Geophysical Validation, Penhors, France, April 27–30*, pages 61–64, Paris, France. ESA.

Gordon, H., Brown, O. & Jacobs, M. (1975a) Computed relationships between the inherent and apparent optical properties of a flat homogeneous ocean. *Appl. Opt.*, 14(2):417–427.

Gordon, H., Clark, D., Mueller, J. & Hovis, W. (1980) Phytoplankton Pigments from the Nimbus–7 Coastal Zone Color Scanner: Comparisons with Surface Measurements. *Science*, 210:63–66.

Gordon, H. & Morel, A. (1983) *Remote assessment of ocean color for interpretation of satellite visible imagery. A review.* Lecture Notes on Coastal and estuarine studies. Springer-Verlag. R. Barber, C. Mooers, M. Bowman, & B. Zeitzschel (eds.).

Gordon, H. R., Brown, O. B. & Jacobs, M. M. (1975b) Computed relationships between inherent and apparent optical properties of a flat homogeneous ocean. *Appl. Optics*, 14:417–427.

Graber, H. C., Thompson, D. R. & Carande, R. E. (1996) Ocean surface features and currents measured with synthetic aperture radar interferometry and HF radar. *Journal of Geophysical Research*, 101(C11):25 813–25 832.

Guillaume, A. & Mognard, N. M. (1992) A new method for the validation of altimeter-derived sea state parameters with results from wind and wave models. *Journal of Geophysical Research*, 97(C6):9705–9717.

Günther, H., Lionello, P. & Hanssen, B. (1993) The impact of the ERS-1 altimeter on the wave analysis and forecast. Technical report, GKSS, Geesthacht, Germany.

Harwar, M. D., Malthus, T. J., Dekker, A. G. & Trueman, I. C. (1995) Reflectance from inland waters: modelling the effects of varied non-living suspended sediment concentration on the spectral features attributed to chlorophyll A. In *RSS95—21$^{st}$ Annual Conference of the Remote Sensing Society*, pages 466–473, Southampton. P. J. Curran and C. Robertson.

Hasselmann, K. & Hasselmann, S. (1991) On the nonlinear mapping of an ocean wave spectrum into a SAR image spectrum and its inversion. *Journal of Geophysical Research*, 96(C6):10 713–10 729.

Hasselmann, K. & Shemdin, O. H. (1982) Remote sensing experiment MARSEN. *International Journal of Remote Sensing*, 3:139–361.

Hesselmans, G. H. F. M. (1996) ERS-1 SAR survey Slijkgat, Slijkgeul and Loswal Noord. Technical Report A011, ARGOSS.

Ikeda, M. & Dobson, F. W., editors. (1995) *Oceanographic Applications of Remote Sensing.* CRC Press, Boca Raton.

Johannesen, J. A., Digranes, G., Espedal, H., Johannesen, O. M., Samuel, P., Browne, D. & Vachon, P. (1994) *SAR Ocean Feature Catalogue*. ESA Publications Division, ESTEC, Noordwijk, The Netherlands. esa-SP-1174, ISBN 92-9092-133-1.

Johannessen, J. A., Røed, L. P., Johannessen, O. M., Evensen, G. Hackett, B., Pettersson, L. H., Haugan, P. M., Sandven, S. & Shuchman, R. (1993) Monitoring and modeling of the marine environment. *Photogrammetric Engineering and Remote Sensing*, 59:351–361.

Johannessen, J. A., Shuchman, R. A., Digranes, G. Lyzenga, D. R., Wackerman, C., Johannessen, O. M. & Vachon, P. W. (1996a) Coastal ocean fronts and eddies imaged with ERS-1 synthetic aperture radar. *Journal of Geophysical Research*, 101(C3):6651–6667.

Johannessen, J. A., Shuchman, R. A., Johannessen, O. M., Davidson, K. L. & Lyzenga, D. R. (1991) Synthetic aperture radar imaging of upper ocean circulation features and wind fronts. *Journal of Geophysical Research*, 96(C6):10 411–10 422.

Johannessen, J. A., Vachon, P. W. & Johannessen, O. M. (1994) ERS-1 SAR imaging of marine boundary layer processes. *Earth Observation Quarterly*, (46):1–5.

Johannessen, O. M. (1986) Brief overview of the physical oceanography. In *The Nordic Seas*, chapter 4, pages 103–127. Springer-Verlag, New York.

Johannessen, O. M., Bjørgo, E., Pettersson, L. H., Sandven, S., Korsbakken, E., Jenkins, A. D., Samuel, P., Evensen, G., Espedal, H. & Hamre, T. (1996b) Proposed strategy for the use of satellite remote sensing in EuroGOOS. In EuroGOOS, editor, *First Intl Conf. on EuroGOOS, October 7-11, The Hague, The Netherlands*, pages 93–114.

Johannessen, O. M., Johannessen, J. A., Jenkins, A. D., Davidson, K., Lyzenga, D. R., Shuchman, R., Samuel, P., Espedal, H. A., Knulst, J., Dano, E. & Reistad, M. (1996c) COAST WATCH-95: ERS-1/2 SAR applications of mesoscale upper ocean and atmospheric boundary layer processes off the coast of Norway. In *Proceedings of IGARSS'96, Lincoln, Nebraska, U.S.A., May 27-31*.

Johannessen, O. M., Korsbakken, E., Samuel, P., Jenkins, A. D. & Espedal, H. A. (1996d) Coast Watch: using SAR imagery in an operational system for monitoring coastal currents, wind, surfactants, and oil spills. In *Proc. EuroGOOS, 7-11 October*, The Hague, The Netherlands.

Johannessen, O. M. and Mork, M. (1979) Remote sensing experiment in the Norwegian coastal waters. Technical Report 3/79, Geophysical Institute, University of Bergen.

Johannessen, O. M., Pettersson, L. H., Johannessen, J. A., Haugan, P. M., Olaussen, T. & Kloster, K. (1989) NORSMAP – Norwegian Remote Sensing Spectroscopy for Mapping and Monitoring of Algal Blooms and Pollution. In *EARSeL Symposium*, Espoo, Helsinki, Finland.

Kerbaol, V., Chapron, B., El Fouhaily, T. & Garello, R. (1996) Fetch and wind dependence of SAR azimuth cutoff and higher order statistics in a Mistral wind case. In IGARSS, editor, *Proceedings of IGARSS'96, Lincoln, Nebraska, U.S.A., 1996 May 27-31*, Pisacataway, New Jersey. IEEE.

Kirk, J. (1981) Monte Carlo study of the nature of the underwater light field in, and the relationships between optical properties of, turbid yellow waters. *Aust. J. Mar. Freshwater Res.*, 32:517–532.

Kirk, J. (1983) *Light and Photosynthesis in Aquatic Ecosystems.* Cambridge University Press.

Komen, G. J., Cavaleri, L., Donelan, M. A., Hasselmann, K., Hasselmann, S. & Janssen, P. A. E. M. (1994) *Dynamics and Modelling of Ocean Waves.* Cambridge University Press.

Korsbakken, E. (1996) Quantitative wind field retrievals from ERS SAR images. Technical report, Ocean and Sea Ice Unit, Earth Sciences Division, ESTEC, ESA.

Korsbakken E. & Johannessen, J. A. (1996) Quantitative wind field retrievals from ERS SAR images. In *Proceedings of the Third ERS Workshop, IFREMER/BREST, 1996 June 18–20.*

Krogstad, H. E., Samset, O. & Vachon, P. W. (1994) Generalizations of the nonlinear ocean–SAR transformation and a simplified SAR inversion algorithm. *Atmosphere–Ocean*, 32(1):61–82.

Lasnier, P., Loeul, S., Hajji, H., Bonicel, D. & Charriez, P. (1996) Contribution of ERS data to Cliosat project, The Satellite Metocean Atlas. In *Proc. Second ERS Applications Workshop, London, 6-8 December, 1995*, number ESA SP-383, pages 65–73. ESA Publications Division, Noordwijk, The Netherlands.

Laur, H., Bally, P., Meadows, P., Sanchez, J., Schaettler, B. & Lopinto, E. (1996) Derivation of the backscattering coefficient $\sigma^0$ in ESA ERS SAR PRI products, 1996. Document No. ES-TN-RS-PM-HL09, Issue 2, Rev. 2, ESA ESRIN.

Laur, H., Meadows, P., Sanchez, J. I. & Dwyer, E. (1993) ERS-1 radiometric calibration. Technical report, ESA ESRIN, Frascati, Italy.

Le Meur, D., Roquet, H. & Lefèvre, J.-M. (1996) Use of ERS wind and wave data for numerical wave modelling at Météo-France. In *Proc. Second ERS Applications Workshop, London, 6-8 December, 1995*, number ESA SP-383, pages 53–56. ESA Publications Division, Noordwijk, The Netherlands.

Lipa, B. J. & Barrick, D. E. (1986) Tidal and storm-surge measurements with single-site CODAR. *IEEE J. ocean. Engng*, OE-11(Special Issue. 2):241–245.

Lyzenga, D. (1978) Passive remote sensing techniques for mapping water depth and bottom features. *Appl. Opt.*, 17:379–383.

Lyzenga, D. (1981) Remote sensing of bottom reflectance and water attenuation parameters in shallow water using aircraft and landsat data. *Int. J. Remote Sensing.*, 1(2):71–82.

Lyzenga, D. R. (1991) Synthetic aperture radar imaging of ocean circulation features and wind fronts. *Journal of Geophysical Research*, 96:10 411—10 422.

Lyzenga, D. R. & Bennett, J. R. (1991) Full-spectrum modeling of SAR internal wave signatures. *Journal of Geophysical Research*, 93(C10):12 345–12 354.

MacArthur, J. L., Marth, J. P. C. & Wall, J. G. (1987) The GEOSAT radar altimeter. *Applied Physics Laboratory Tech. D.*, 8(2):176–181.

Mangolini, M., Ranchin, T. & Wald, L. (1994) Methods and device for increasing the spatial resolution of images from other images of better spatial resolution. USA patent serial 08/249,882.

Maritorena, S. & Guillocheau, N. (1996) Optical properties of water and spectral light absorption by living and non-living particles and by yellow substances in coral reef waters of French Polynesia. *Marine Ecology Progress Series*, 131:245–255.

Maritorena, S., Morel, A. & Gentili, B. (1994) Diffuse reflectance of oceanic shallow waters: Influence of water depth and bottom albedo. *Limnol. Oceanogr.*, 39(7):1689–1703.

Meadows, P. J. & Willis, C. J. (1995) Derivation of radar cross section coefficient in UK-PAF ERS-1.SAR.PRI products. Technical report, GEC-MARCONI Research Centre.

Mishra, A., Sridhar, P. & Prasad. K. (1989) Bathymetry retrieval algorithm for coastal water (case II) from Landsat-5 Thematic Mapper data. In *IGARSS'89: 12th Canadian Symp. Remote Sensing*, Vancouver, Canada.

Mobley, C., Gentili, B. Gordon, H., Jin, Z., Kattawar, G., Morel, A., Reinersman, P., Stamnes, K. & Stavn, R. (1989) Comparison of numerical models for computing underwater light fields. *Appl. Opt.*, 32(36):7484–7504.

Monaldo, F. (1988) Expected differences between buoy and radar altimeter estimates of wind speed and significant wave height and their implications on buoy–altimeter comparisons. *Journal of Geophysical Research*, 93(C3):2285–2302.

Monaldo, F. M. (1991) The consequences of sampling variability on the estimation of wave number and propagation direction from spaceborne SAR image spectra. *IEEE Transactions on Geoscience and Remote Sensing*, 29(1).

Morel, A. (1988) Optical Modeling of the Upper Ocean in Relation to Its Biogenous Matter Content (Case I Waters). *J. Geophys. Res.*, 93(C9):10749–10768.

Morel, A. & Prieur, L. (1977) Analysis and variations in ocean color. *Limnol. Oceanogr.*, 22:709–722.

NOAA. (1995) NOAA polar orbiter data user's guide. http://www2.ncdc.noaa.gov/POD/.

Paci, G. & Campbell, G. (1996) Operational use of ERS-1 products in marine applications. In ESA, ESA (1996), pages 43–46.

Pettersson, L. H. (1990) Application of remote sensing to fisheries. Vol.1. Technical Report EUR 12867 EN, Commission of the European Communities, Joint Research Centre, Ispra, Italy.

Pettersson, L. H. (1995) Remote sensing of Coccolithophorid blooms: The European *emiliania huxleyi* programme—EHUX. Final report to CEC under contract MAST-CT92-0038, CEC. Edited by R. Morris.

Pettersson, L. H. & Skrøvseth, P. E. (1992) Development and implementation of a SeaWIFS application program in Norway. In *First Thematic Conf. on Remote Sens. for Marine & Coastal Environments, New Orleans, Louisiana*, U.S.A.

Platt, T. & Sathyendranath, S. (1988) Oceanic primary production: Estimation by remote sensing at local and regional scales. *Science*, 241:1613–1620.

Platt, T. & Sathyendranath, S. (1988) Biological Production Models as Elements of Coupled, Atmosphere-Ocean Models for Climate Research. *J. Geophys. Res.*, 96(C2):2585–2592.

Platt, T. & Sathyendranath, S. (1993) Estimators of primary production for interpretation of remotely sensed data on ocean color. *J. Geophys. Res.*, 98(C8):14561–14576.

Platt, T., Sathyendranath, S., Caverhill, C. M. & Lewis, M. (1988) Ocean primary production and available light: further algorithms for remote sensing. *Deep-Sea Research*, 35(6):855–879.

Polcyn, F. & Sattinger, I. (1969) Water depth determinations using remote sensing techniques. In *6th International Symp. on Remote Sensing of Environment*, pages 1017–1028. ERIM.

Pospelov, M. N. (1996) Surface wind speed retrieval using passive microwave polarimetry: The dependence on atmospheric stability. *IEEE Transactions on Geoscience and Remote Sensing*, 34(5): 1166–1171.

Prandle, D. (1991) A new view of near-shore dynamics based on HF radar. *Progress in Oceanography*, 27:403–438.

Preisendorfer, R. W. (1961) Application of radiative transfer theory to light measurements in the sea. *Union Geod. Geophys. Int. Mon.*, 10:11–29.

Prieur, L. & Sathyendranath, S. (1981) An optical classification of coastal and oceanic waters based on the specific spectral absorption curves of phytoplankton pigments, dissolved organic matter, and other particulate material. *Limnol. Oceanogr.*, 26:671–689.

Puls, W., Doerffer, R. & Sündermann, J. (1994) Numerical simulation and satellite observations of suspended matter in the North Sea. *IEEE J. Oceanic Eng.*, 19:3–9.

Ranchin, T. (1994) Efficient data fusion using wavelet transform: the case of spot satellite images. In SPIE, editor, *Proc. SPIE's 1993 Int. Symp. Optics, Imaging and Instrumentation*, volume 2034, pages 171–178. SPIE.

Romeiser, R. (1993) Global validation of the wave model WAM over a one year period using GEOSAT data. *Journal of Geophysical Research*, C98:4713–4726.

Rufenach, C. L. & Alpers, W. R. (1978) Measurement of ocean wave heights using the GEOS 3 altimeter. *Journal of Geophysical Research*, 83:5011–5018.

Samuel, P., Johannessen, J. A. & Johannessen, O. M. (1994) A study on the inflow of Atlantic water to the GIN Sea using GEOSAT altimeter data. In *The Polar Oceans and Their Role in Shaping the Global Environment*, pages 95–108. Americal Geophysical Union.

Sathyendranath, S., Hoge, F., Platt, T. & Swift, R. (1994) Detection of phytoplankton pigments from ocean color: improved algorithms. *Appl. Opt.*, 33(6):1081–1089.

Sathyendranath, S., Platt, T., Caverhill, C. M., Warnock, R. & Lewis, M. R. (1989) Remote sensing of ocean primary production: computations using a spectral model. *Deep-Sea Research*, 36(3): 431–453.

Sathyendranath, S., Prieur, L. & Morel, A. (1987) An evaluation of the problems of chlorophyll retrieval from ocean color, for Case 2 waters. *Advances in Space Research*, 7.

Scoon, A., Robinson, T. S. & Meadows, P. J. (1996) Demonstration of an improved calibration scheme for ERS-1 SAR imagery using a scatterometer wind model. *International Journal of Remote Sensing*, 17(2):413–418.

Shay, L. K., Graber, H. C., Ross, D. B., Chemi, L., Peters, N., Hargrove, J., Vakkayil, R. & Chamberlain, L. (1996) Measurement of ocean surface currents using an HF radar during HIRES-2. Technical Report 93-007, Rosenstiel School of Marine and Atmospheric Sciences, University of Miami.

Shemer, L. (1993) Interferometric SAR imagery of a monochromatic ocean wave in the presence of the real aperture radar modulation. *International Journal of Remote Sensing*, 14(16):3005–3019.

Skofronick-Jackson, G. M. & Gasiewski, A. J. (1995) Nonlinear statistical retrievals of ice content and rain rate from passive microwave observations of a simulated convective storm. *IEEE Transactions on Geoscience and Remote Sensing*, 33(4):957–970.

Smith, S. D. (1988) Coefficients for sea surface wind stress, heat flux and wind profiles as a function of wind speed and temperature. *Journal of Geophysical Research*, 93(C12):15 467–15 472.

Stanev, E. V. (1994) Assimilation of sea surface temperature data in a numerical ocean circulation model. A study of the water mass formation. In P. P. Brasseur & J. C. J. Nihoul, editors, *Data Assimilation: Tools for Modelling the Ocean in a Global Change Perspective*, volume 119 of *NATO ASI*, pages 33–58. Springer-Verlag Berlin Heidelberg.

Stoffelen, A. C. M. & Anderson, D. L. T. (1993) ERS-1 scatterometer data characteristics and wind retrieval skill. In *Proc. First ERS-1 Symposium, Space at the Service of Our Environment, Cannes, France, 1992 November 4-6*. ESA SP-359.

Tanis, F., Bennett, J. & Lyzenga, D. (1989) *Physics of EOM*. Technical Report No. 028, ERIM.

Tassan, S. (1988) The effect of dissolved yellow substance on the quantitative retrieval of chlorophyll and total suspended sediment concentrations from remote measurements of water colour. *Int. J. Remote Sensing.*, 9(4):787–797.

Tassan, S. & d'Alcala, M. R. (1993) Water quality monitoring by Thematic Mapper in coastal environments. A performance analysis of local biooptical algorithms and atmospheric correction procedures. *Remote Sens. Environ.*, 45:177–191.

Tassan, S. & Sturm, B. (1986) An algorithm for the retrieval of sediment content in turbid coastal waters from CZCS data. *Int. J. Remote Sensing.*, 7(5):643–655.

Vachon, P. W. & Dobson, F. W. (1996) Validation of wind vector retrieval from ERS-1 SAR images over the ocean. The Global Atmosphere–Ocean System (in press).

Vachon, P. W., Johannessen, J. A. & Browne, D. (1995) ERS-1 SAR images of atmospheric gravity waves. *IEEE Transactions on Geoscience and Remote Sensing*, 33(4):1014–1025.

Vos, R. & Schuttelaar, M. (1995) RESTWAQ, Data assessment, data-model integration and application to the southern North Sea. Technical Report 95-19, BCRS, Delft, The Netherlands.

Vos R. J., *et al.* (1997) The combined use of remote sensing imagery and water quality models in the southern North Sea. In *Fourth Intl Conf on Remote Sensing for Marine and Coastal Environments, Florida, USA, 17–19 March*, volume 2, page 23.

Wackerman, C., Rufenach, C., Shuchman, R. A. & Johannessen, J. A. (1995) Wind field retrievals from ERS-1 SAR. Submitted to *J. geophys. Res.*

Wackerman, C., Rufenach, C., Shuchman, R. A., Johannessen, J. A. & Davidson, K. (1996) High resolution wind retrieval using ERS-1 synthetic aperture radar imagery. IEEE (in press).

Wald, L., Ranchin, T. & Mangolini, M. (1997) Fusion of satellite images of different resolution: Assessing the quality of resulting images. *Photogram. Eng. Remote Sensing*, 63(6):691–699.

Witter, L. D. & Chelton, B. D. (1991) A GEOSAT altimeter wind speed algorithm and a method for altimeter wind speed algorithm development. *Journal of Geophysical Research*, 96(C5): 8853–8860.

Woods, J., Dahlin, H., Droppert, L., Glass, M., Vallerga, S. & Flemming, N. (1996) The strategy for EuroGOOS. EuroGOOS publication No. 1, Southampton Oceanography Centre, Southampton. ISBN 0-904175-22-7.

Wu, J. (1993) Ripples and oceanic remote sensing. In *Proc. Environment'93*. HKUST, Hong Kong.

Wu, X., Flather, R. A. & Wolf, J. (1994) A third generation wave model of European continental shelf seas, with depth and current refraction due to tides and surges and its validation using GEOSAT and buoy measurements. Technical Report 33, Proudman Oceanographic Laboratory, Birkenhead, U.K.

Xia, L. (1993) A united model for quantitative remote sensing of suspended sediment concentration. *Int. J. Remote Sensing.*, 14(14):2665–2676.

# Appendix A:  Verification of waves in the Spanish data set with altimeter data from TOPEX/POSEIDON

# PROMISE project: Verification of the waves in Spanish Data Set with altimeter data from the TOPEX/POSEIDON satellite

Marta Gómez Lahoz, Juan Carlos Carretero

Clima Marítimo

December 1996

Since November 95, an operational wave forecasting system is being run by the Spanish Holding of Harbours (CM - Puertos del Estado (PE)), the forecasting system is based on the WAM model Cycle 4 driven by wind fields supplied by "Oceanweather Inc.". The standard version of the WAM model has been modified by PE in order to introduce a two-way nesting scheme which, in practice, works as a variable grid spacing scheme. The application developed in such a way for the North Atlantic Ocean has a resolution that goes from 3° down to 0.25° at the coast of Spain (Figure 1). This wave forecast is routinely verified against data from the Spanish coastal buoys. The analyzed waves archived by the system for the period November 95 to March 96 are going to be included as a part of the Spanish Data Set which is in preparation for the PROMISE project, this data set covers the Bay of Biscay.

Alastair Jenkins, from the Nansen Environmental and Remote Sensing Centre (NERSC), has supplied, within the frame of the PROMISE project, a file prepared by Paul Samuel and Vibeke Jensen (NERSC) with altimeter data from the TOPEX/POSEIDON to verify the wind and wave data in open waters in the area covered by the data set. From the several tracks supplied to PE (Figure 2), a subset was extracted according to the following considerations: the time mismatch between the measurement along the track and the model output was set to a maximum of one hour, and from all the possible tracks, the nearest to the bay were chosen. In this summary, the tracks for which high waves were measured (figures 4 to 11) are shown.

Figure 3 shows a scatter plot of the total sample, around 5000 pairs of values. The overall agreement is good, although it is evident that the geophysical variability of Hs is measured by the satellite, and can not be reproduced by the model, this variability is probably related to wind variability. Table 1 shows a summary of the statistical analysis of the comparison of all the tracks. No significant bias is present in the comparison and the values for the RMSE and correlation are quite good. The values for the regression slope and interception indicate some underestimation of high waves by the model. The fact that a buoy measurement significantly filters this geophysical variability when measuring during 30 minutes or mores, leads to the fact that the values for the statistical parameters obtained from this type of comparison are of different nature to those obtained when comparing with a buoy.
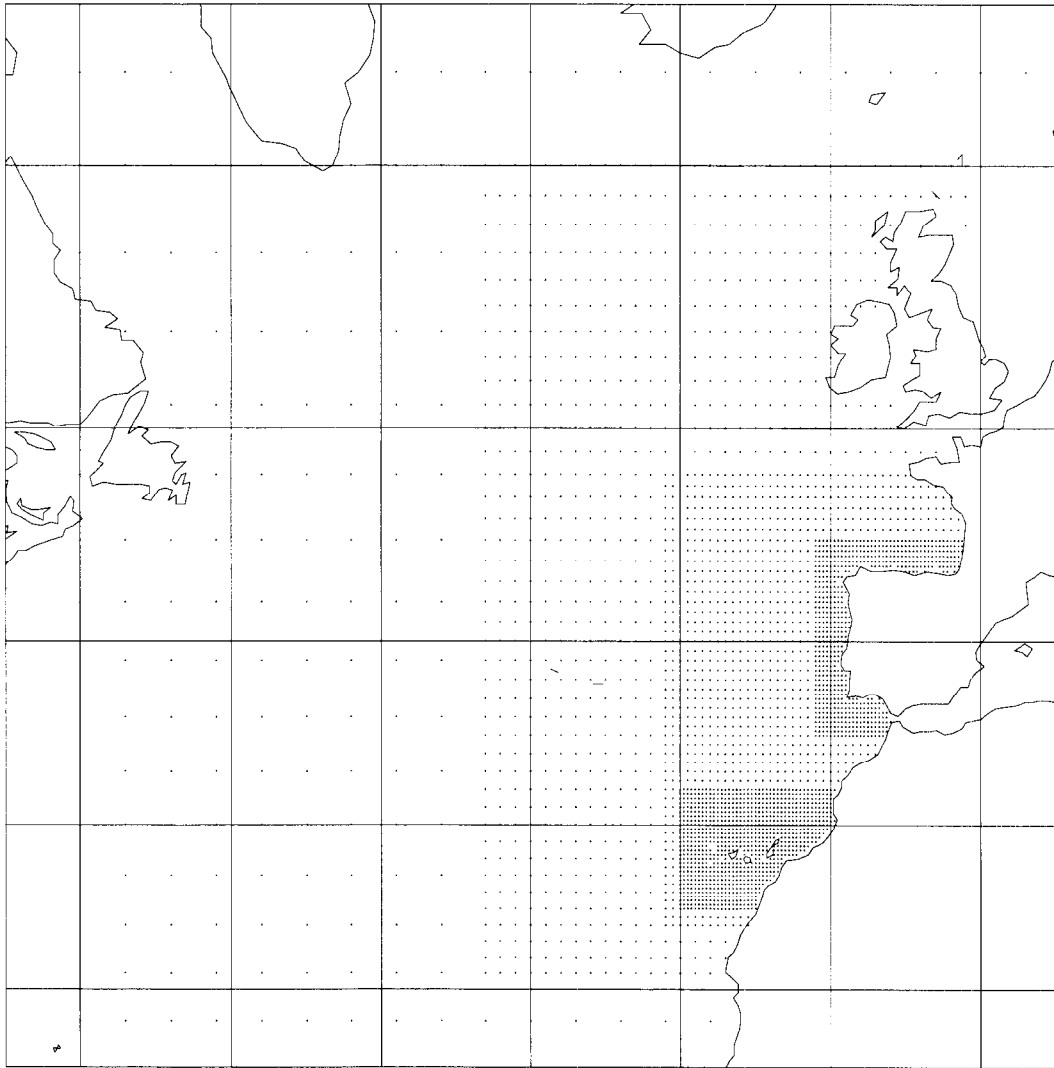
Figure 1: WAM grid for the Atlantic Coast of Spain. The resolution goes from 3°
down to 0.25° in the coast.
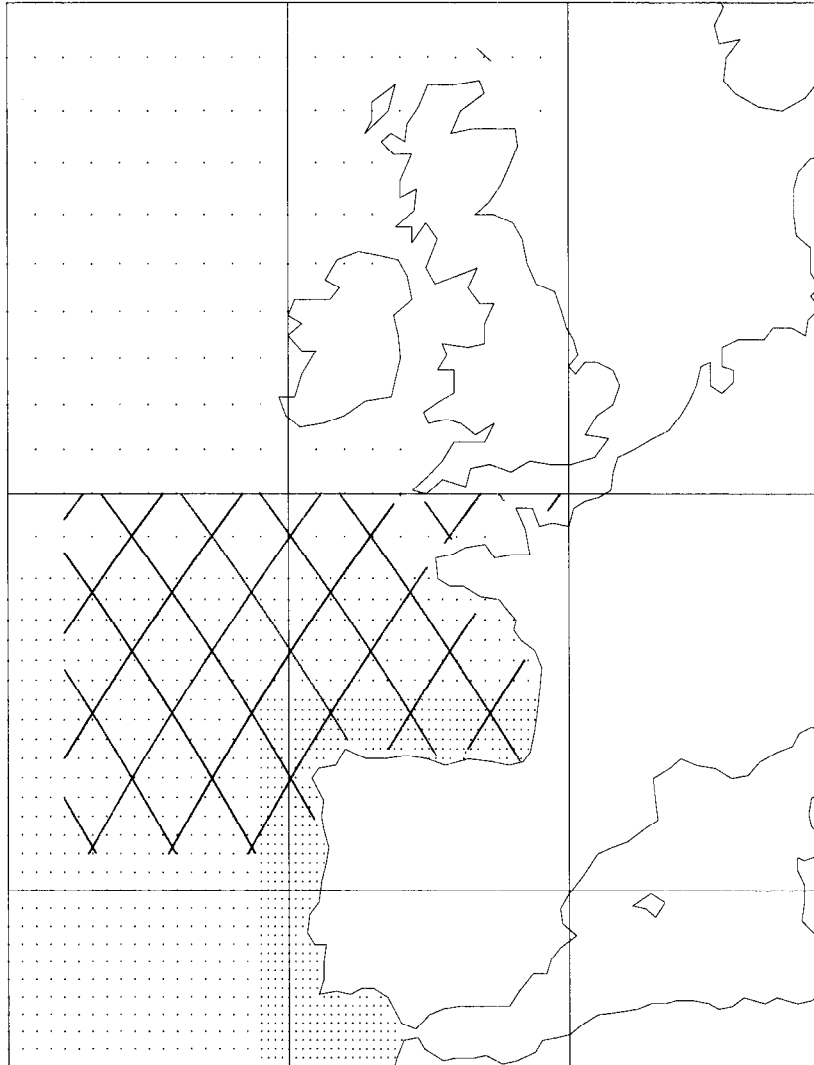
Figure 2: Tracks from the TOPEX/POSEIDON satellite in the area of the Bay of Biscay.
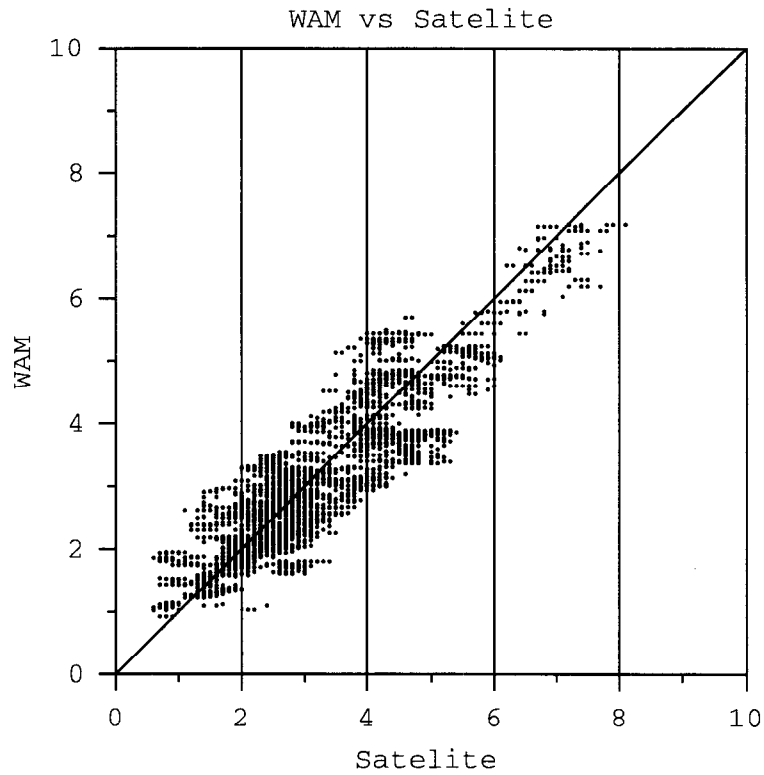
Figure 3: Scatter plot of model waves versus altimeter data for the analyzed period.

```
TABLE 1 : Verification of WAM output with altimeter data. Summary of wave deviations.
|---------------------------------------------------------------------------------|
| CLASS INT |SAMPLE| MEAN S | MEAN W |  CORR  |SLOPE| INT | RMSE  |  BIAS  |  SI    |
|---------------------------------------------------------------------------------|
|  TOTAL     4916 |  3.066    3.008    0.890   0.82  0.51  0.586   -0.057    0.191 |
|---------------------------------------------------------------------------------|
```
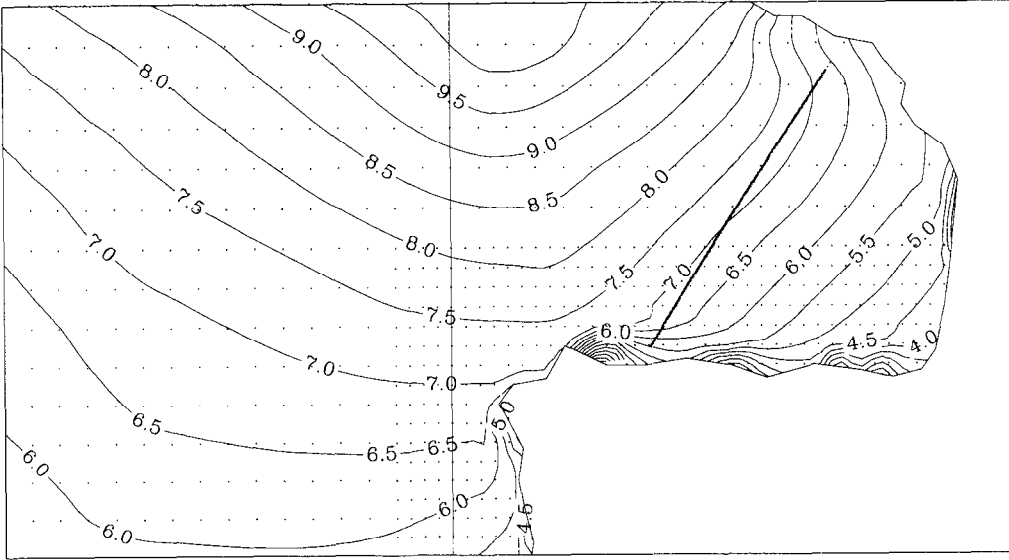
Figure 4: Hs contour map for the 10th of Feb 96. The satellite track is shown superimposed to the WAM output.
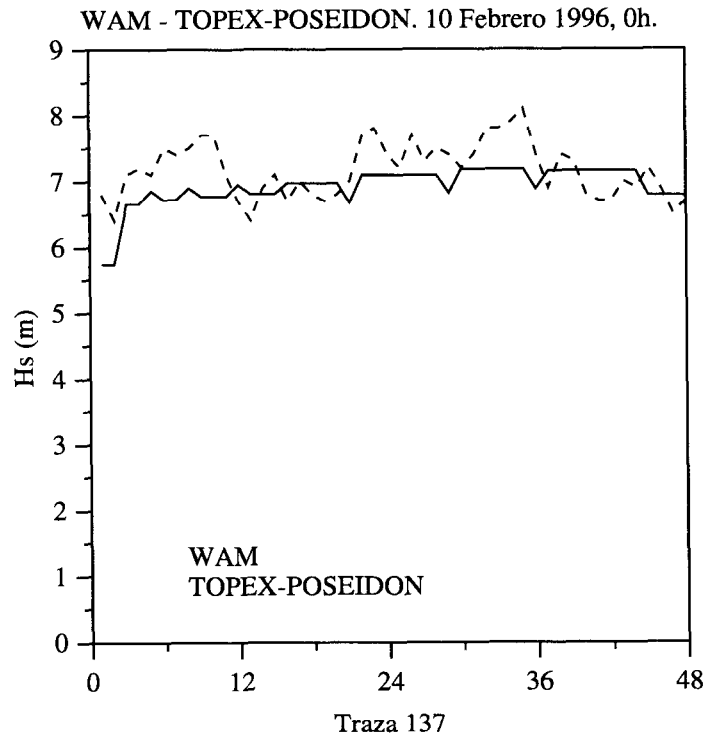


Figure 5: Hs measured by the satellite along the track shown in figure 4.
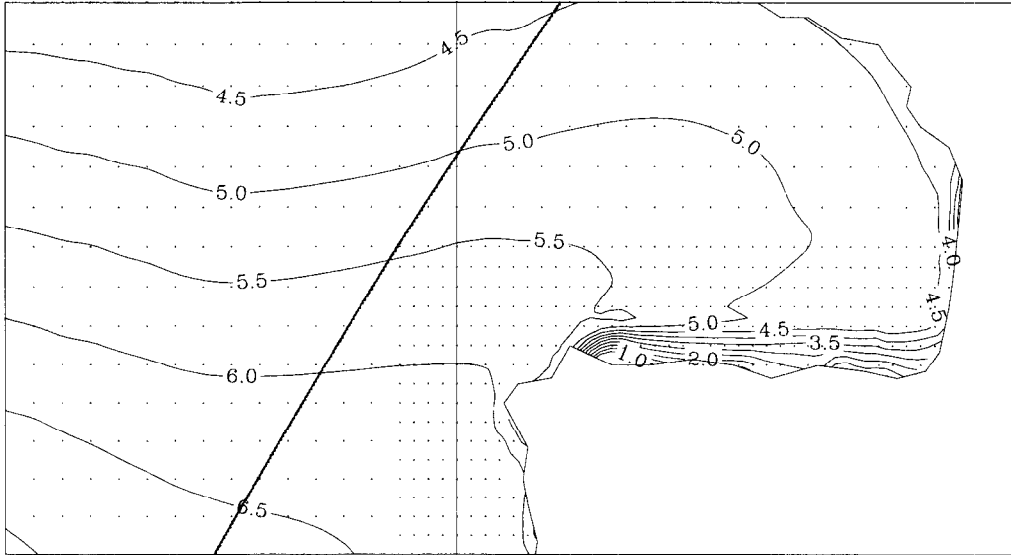
Figure 6: Hs contour map for the 15th of Jan 96. The satellite track is shown superimposed to the WAM output.
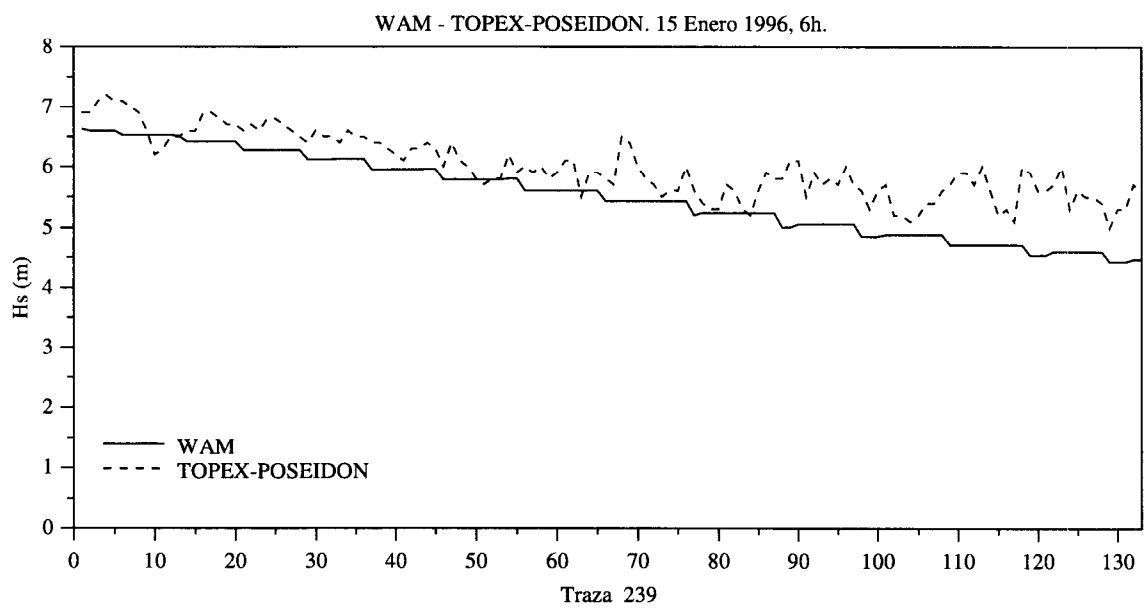


Figure 7: Hs measured by the satellite along the track shown in figure 6.
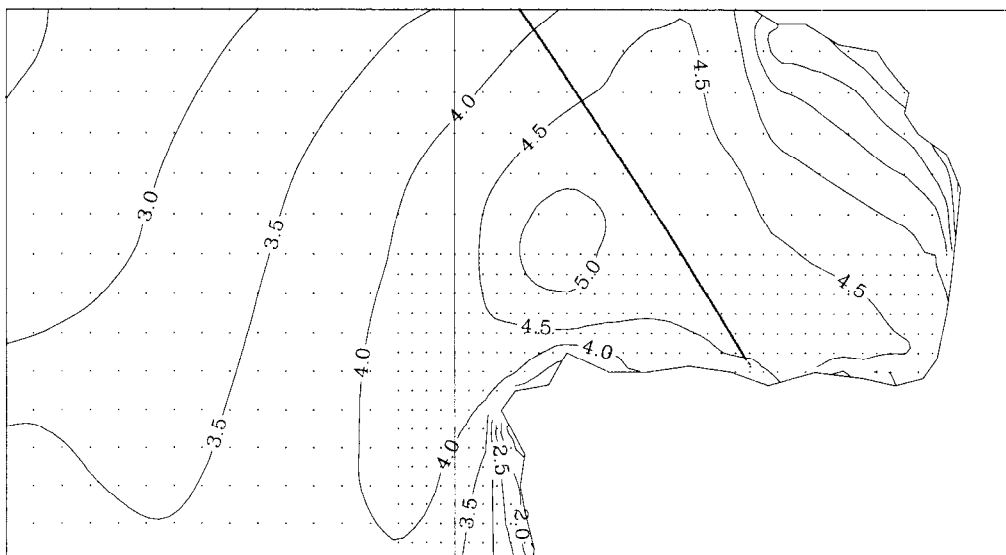
Figure 8: Hs contour map for the 21st of Feb 96. The satellite track is shown superimposed to the WAM output.
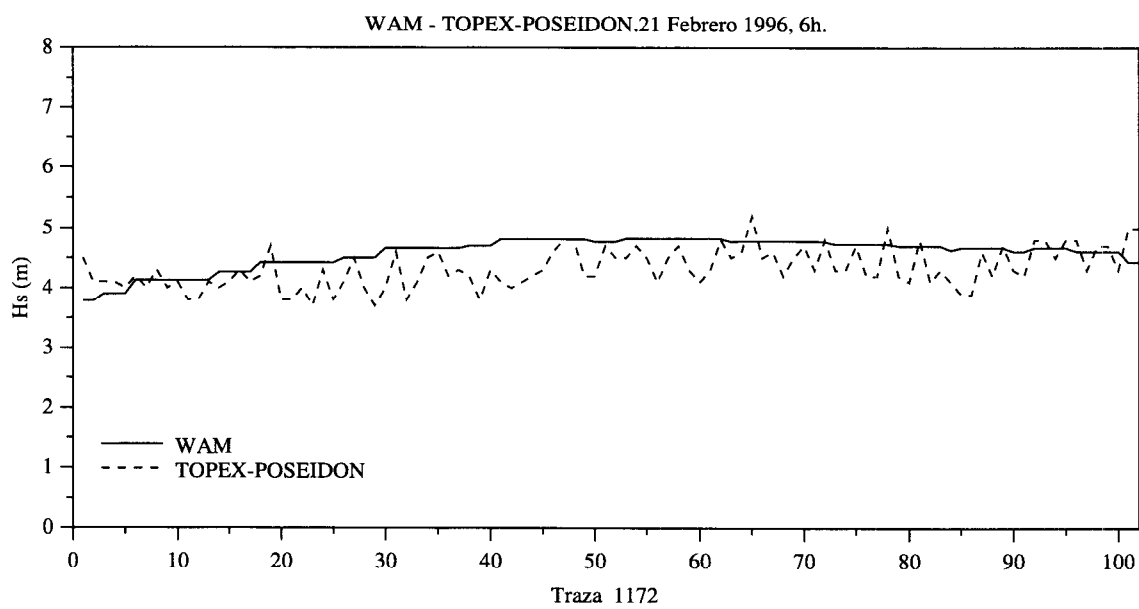


Figure 9: Hs measured by the satellite along the track shown in figure 8.
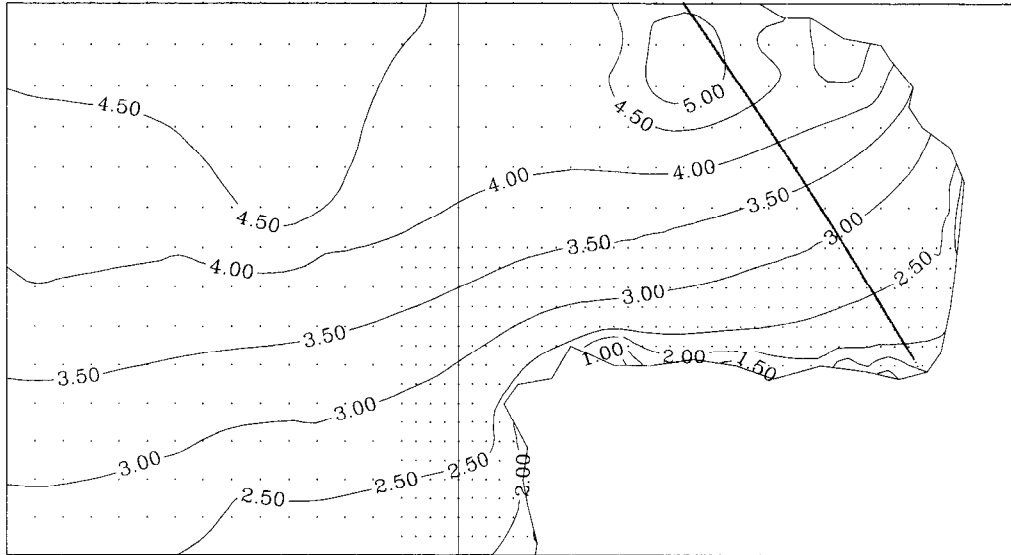
Figure 10: Hs contour map for the 24th of Feb 96. The satellite track is shown superimposed to the WAM output.
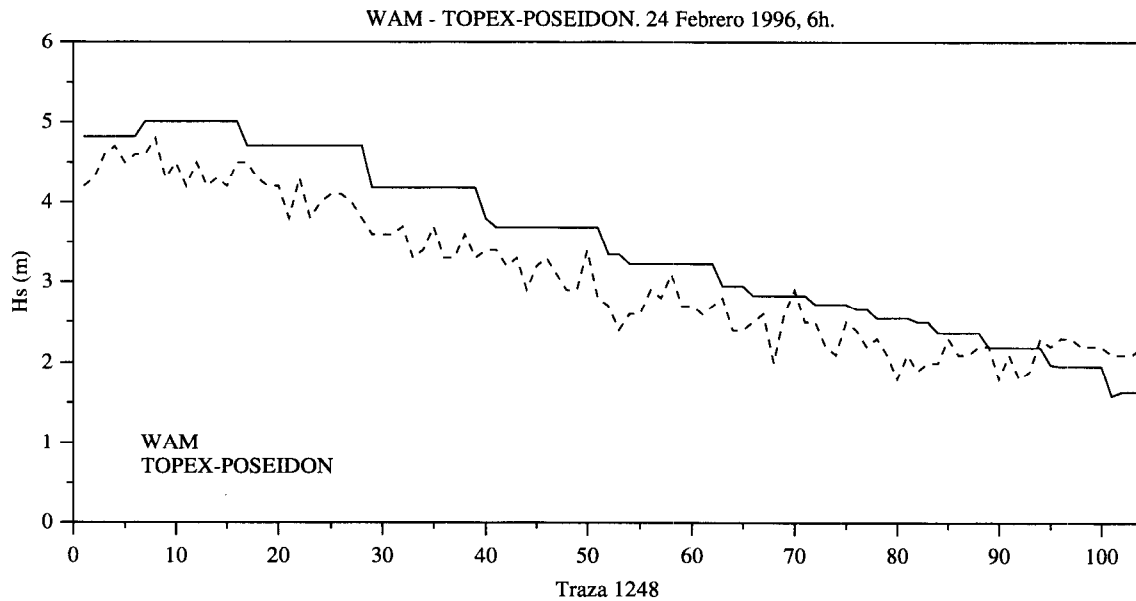


Figure 11: Hs measured by the satellite along the track shown in figure 10.

# Appendix B: Use of NOAA/AVHRR satellite remote sensing data for modelling suspended sediment transport

# Use of NOAA/AVHRR satellite Remote Sensing data

# for modelling of

# suspended sediment transport in the North Sea

by

**Robert J. Vos**

**and**

**Herman Gerritsen**

Delft Hydraulics, The Netherlands

Z2025

January 1997

**Table of Contents:**

**List of Figures:**

## 1. Introduction

This document addresses the use of NOAA /AVHRR satellite Remote Sensing data for modelling of suspended sediment transport within the framework of the MAST3 joint research project PROMISE (contract MAS3-CT95-0025), as envisaged by Delft Hydraulics. The primary focus of Delft Hydraulics' activities in PROMISE is sediment modelling in the North Sea, both on regional scale and local scale, and the combination of model and remote sensing data and sensitivity analysis using structured data-assimilation procedures (Gerritsen and Vos, 1996).

The present document is a background or status document, in the sense that it gives an overview of the remote sensing data sources and the processing and conversions required (Chapter 2), followed by a description of the available data and the structured formal procedure to combine NOAA/AVHRR images with a water quality model, developed by Vos and Schuttelaar (1995) in an earlier study (Chapter 3). Chapter 4 contains a summary and conclusions.

The document forms Appendix B to the PROMISE project Report "Remote Sensing applied to Operational Modelling", being prepared by the PROMISE participants, January 1997. It also appears as a separate research report, with the same title and authors (Delft Hydraulics' Report Z2025, January 1997).

## 2. Data and sensors required for operational modelling of Total Suspended Matter

### 2.1 In-situ data and Remote Sensing data for operational modelling

Traditionally water quality models of suspended matter are calibrated on in-situ data. Unfortunately, in-situ data have several shortcomings:

- for large marine systems such as the North Sea, they cover only a very limited area;

- for parameters like Total Suspended Matter (TSM) that have a "patchy" spatial distribution, in-situ data give very little information on patterns of TSM. Interpolation techniques like kriging are known for their failure to reproduce TSM patterns;

- In-situ data on suspended matter have a large natural variability in time. This makes that in-situ data should be sampled by continuous monitoring in order to assess and minimize its variability effects. If this is not the case, in-situ data should be used with large error margins;

These shortcomings can partially be countered by using Remote Sensing satellite imagery. Characteristics of Remote Sensing data are:

- remote rensing data are synoptic. Especially patterns on TSM render valuable additional information on the patchy spatial variations

- the spatial resolution of the sensor effectively leads to integration of small scale spatial variability. For instance, for the NOAA/AVHRR satellite the spatial resolution is a pixel size of $1.1*1.1$ km$^2$.

- The sampling in time is variable and generally low. Some of the satellites present images with a high frequency, though, sometimes even on a daily basis;

An important disadvantage of the use of Remote Sensing images for TSM is that they require correction of atmospheric disturbance and sea surface glint. Correction procedures have a large impact, since firstly about 80% of the signal should be corrected for these effects, and secondly sea surface glint and aerosol scattering are hard to correct for.
Stated simply: Without any correction procedure the Remote Sensing images are of little value.

Reliable correction procedures are therefore of prime importance for the use of Remote Sensing data. The present report and section describes only images that have already been corrected for using reliable and well described procedures, e.g. those used by the Royal Netherlands Meteorological Institute (KNMI), see Prangsma and Roozekrans (1989, 1992).

At first glance a further disadvantage of Remote Sensing images for TSM applications is the fact that only the surface layer (one to a few meters) is sampled by the sensor. Nevertheless, for the calibration of computational models - viz. the ones that resolve the vertical - this information is still very useful.

## 2.2 Suitability of sensors for operational monitoring of water quality parameters

### 2.2.1 The NOAA/AVHRR satellite

Remotely sensed information in the visible spectrum can generally be used to analyze the spatial distribution of three water quality parameters, namely yellow substance, phytoplankton and silt. The NOAA/AVHRR satellite has only one usable Channel (580-680 nm) in the visible part of the light spectrum. Therefore this satellite can not be used to partition the TSM fraction into an inorganic fraction (e.g. silt) and an organic one (e.g. phytoplankton and detritus). Fortunately, for the Southern North Sea the contribution of the organic fraction to the reflectance in satellite images is generally low, so TSM information derived from NOAA/AVHRR images for these waters mainly corresponds with silt.
For the northern part of the North Sea where the silt concentration can be very low (< 2mg/l) and algae blooms may occur frequently this is certainly not the case. In these waters there may be a serious problem to relate TSM to either the inorganic or the organic fraction. We note that the NOAA/AVHRR satellite can not be used to analyze yellow substance.

### 2.2.2 Comparison with other satellites

An important advantage of the NOAA/AVHRR satellite over other satellites is that two images of the North Sea are obtained every day. A high frequency is important since in the North Sea cloud cover reduces the amount of usable information significantly. The frequency of passage of other satellites like LANDSAT/TM or SPOT is therefore far from adequate. Furthermore the information obtained from these satellites is of too small a scale and too detailed for studying large marine systems. The combination of information from several satellites may be promising. At the moment, such an approach may easily lead to very high costs. Some of the SPOT images are useful for detailed study of processes in crucial local areas of the North Sea (e.g. Dover Strait).

Data from the Coastal Zone Colour Scanner (CZCS) have been widely used in the past, but can not be used at present since this satellite ended its mission in 1986. Data from the Japanese satellite ADEOS that has recently been launched (August 1996) are not yet available to end-users, and therefore can not be used within the PROMISE project. The new SEAWIFS satellite to be launched in 1997 may equally only provide useful data at a later stage.

So, for the calibration of water quality models on TSM, only the data from the NOAA/AVHRR satellite is presently sufficient in terms of frequency and spatial coverage.

## 2.3 Corrections to NOAA/AVHRR reflection images

### 2.3.1 Data processing at KNMI

In the Netherlands, NOAA/AVHRR products are routinely processed by the Royal Netherlands Meteorological Institute KNMI. KNMI corrects raw imagery of NOAA/AVHRR Channel 1 (580 - 680 nm) for atmospheric scattering, aerosol scattering and sea surface glint by using Channel 2 data (725nm-1100nm). Such a procedure was first developed by Viollier et al. (1980) for CZCS satellite data. It has been adjusted by KNMI for use on NOAA/AVHRR satellite data (Prangsma and Roozekrans, 1989, 1992). Figure 1 shows an example image, taken on 28 June 1995. It shows that, without any cloud cover, the KNMI images cover the North Sea almost completely.

KNMI processes daily NOAA/AVHRR images into weekly composites in order to get an image that maximally covers the North Sea. These NOAA/AVHRR products contain the above water-reflectance $R_\lambda(0+)$, with the $\lambda$ bandwidth 580 - 680 nm.

### 2.3.2 Reflectance

The physical quantity that is related to water quality parameters, however, is the under-water reflectance $R_\lambda(0-)$. The above water-reflectance $R_\lambda(0+)$ is related to the under water-reflectance $R_\lambda(0-)$ by:

$$R_\lambda(0+) = R_\lambda^{surf} + \gamma\ R_\lambda(0-)$$

with:

$\gamma$ = dimensionless conversion factor due to Snell's law

$R_\lambda^{surf}$ = above water reflectance at the water surface due to Fresnel reflectance

$R_\lambda^{surf}$ increases with solar zenith angle, and is smaller for diffuse light than for collimated light. For irregular water surfaces (waves, ripples) Fresnel reflectance may even occur at zero solar zenith angle. Theoretically, for an optically deep (i.e homogeneous) water column, the factor $\gamma$ is given by (Gordon, 1975):

$$\gamma = \frac{1}{n^2 \, T_w}$$

with:

n     = refractive index of sea water
$T_w$     = transmission through the water surface

Krijgsman (1994) reports values for $\gamma$ of 0.52 to 0.562.
In order to get insight in the conversion of Reflectance to TSM concentrations, the under-water Reflectance R(0-) is discussed in more detail.

## 2.3.3 The relation between the under-water Reflectance R(0-) and water quality parameters

For a homogeneous, infinitely deep medium, neglecting fluorescence and Raman Scattering (Gordon et al., 1975; Prieur et al. 1990; Dekker, 1993; Krijgsman 1994; Althuis 1994, Stumpf 1992, and many others) the under water reflectance $R_\lambda(0-)$ for a given wavelength $\lambda$ can be approximated (quoted from Krijgsman, 1994) by:

$$R_\lambda(0-) = r_1 \, \omega_b(\lambda) + r_2 \, \omega_b^2(\lambda) + higher order terms$$

$$\omega_b(\lambda) = \left[ \frac{\sum_i b_b{}^*_i(\lambda)C_i}{a_w(\lambda) + \sum_i a^*_i(\lambda)C_i + \sum_i b_b{}^*_i(\lambda)\,C_i} \right]$$

with:

$r_{(1,2)}$     = coefficients
$\omega_b$     = backscattering albedo
$b_b{}^*_i$     = specific backscattering coefficient (m²/mg) of component i
$C_i$     = concentration (mg/m³) of component i (e.g. phytoplankton or silt)
$a_w$     = absorption coefficient of sea water ($m^{-1}$)
$a^*_i$     = specific absorption coefficient ($m^{-1}$) of component i (e.g. yellow substance, phytoplankton or silt)
$\lambda$     = wavelength (m)

In practice only the first term in this expansion is relevant.

The specific backscattering coefficient $b_b{}^*_i$ is related to the specific scattering coefficient b, by means of the volume scattering function $\beta(\theta)$, with $\theta$ the scattering angle. The volume scattering function $\beta(\theta)$ describes the angular distribution (differential cross section) of the scattering event. Backscattering is that part of the scattering with a scattering angle larger than 90 degrees. Generally, the volume scattering function is accounted for by defining a ratio $\kappa$ between the specific backscattering scattering coefficient and the specific scattering coefficient:

$$\kappa = \frac{b_b^*}{b^*}$$

For Dutch lakes, Dekker finds values of $\kappa$ from 0.017 to 0.047 (Dekker, 1993). A commonly quoted value for $\kappa$ is 0.019 (Kirk, 1991), based on a volume scattering function measured by Petzold (1972). The coefficients $r_i$ are related to solar zenith angle and the volume scattering function ($\beta$), (Kirk, 1991). For a zero solar zenith angle, the absence of diffuse sky light and a flat water surface, $r_1$ is found to be 1/3. For waters with $(a/b_b) > 4$, Kirk finds a linear relationship:

$$R(0-) = 0.331 \frac{b_b}{a}$$

in which:

$b_b$ = total backscattering coefficient $(m^{-1})$
$a$ = total absorption coefficient $(m^{-1})$

Kirk also derived a relation for six different water types for different solar altitudes. The departure of the response of the above given relation from $r_1 = 1/3$ for increasing zenith angles is different for the various water types, but could be related to a parameter $\mu_s$, that is related to the asymmetry of the volume scattering function $\beta(\theta)$ around a scattering angle of 90 degrees. Dekker reports a large spread in $r_1$ (~0.1-0.5), when $r_1$ is calibrated on data for Dutch lakes (Dekker, 1993).

## 2.3.4   The simplied linear model of Vos (1995)

A very simple model for NOAA/AVHRR Channel 1 is presented in (Vos, 1995):

$$R(0+) = R_{back} + 0.178 \left[ \frac{C}{\dfrac{a_w'}{b_b^*} + C} \right]$$

with:

$R_{back}$ = Reflectance- % due to reflectance at the water surface $(R^{surf})$, and atmospheric scattering $(R^{atm})$, in the NOAA/AVHRR Channel 1. So, $R_{back}$ refers to the reflectance-% that does not originate from the water column, and should be corrected for;

$b_b^*$ = average specific back scattering coefficient $(m_{-1}\ l/mg)$ of sediment particles;

$C$ = average concentration $(mg/l)$ of sediment particles;

$a_w'$ = constant absorption coefficient of sea water $(m_{-1})$, possibly including a correction for algae or silt (at high silt concentrations);

Assumptions in this model are:
- there is only one sediment fraction;
- a scattering albedo $\omega_0 < 0.95$;
- a constant adsorption coefficient for the water column;
- a solar zenith angle of zero and $\gamma=.534$;
- a simplification of multiple scattering;
- no Raman Scattering and Fluorescence;
- a 'background' reflectance-% can be determined;

This model satisfies a saturation law for higher levels of C. As noted already by Kirk (1991), for not too high concentrations of scattering material, it may be assumed that $(a'_w/b_b^*) >> C$ and this automatically leads to a linear relation:

$$R(0+) = R_{back} + a'C$$

with:

$R_{back}$ = Reflectance % due to (background) disturbance
$a'$ = 0.178 $b_b^*/a'_w$
$C$ = average concentration (mg/l) of sediment particles

## 2.3.5 Choice of a semi-empirical fit relation for NOAA/AVHRR Channel 1 data

In practice, several semi-empirical relationships have been used to approximate the above given theoretical formulae. These relationships are a linear-regression of TSM (X) against Reflectance (Y), a linear regression of 1/X versus 1/Y or logarithmic regressions like linY-logX and logX-logY (Stumpf R.P., 1992; Marees and Wernand, 1992; Prangsma and Roozekrans, 1989, 1992). The difference between these relations is that some of them describe the saturation law explicitly (logarithmic, inverse or other relation), and others use a simple linear relation that neglects saturation. The argument for using a linear relationship is that the formally better description of the saturated part is not very useful in practice since the small sensitivity of the relationship in this region indicates that Remote Sensing can not be used to analyze TSM in this region.
Therefore, for the sensitive part of the relation a linear relationship is established, while the saturated part of the relation is simply neglected.

In the RESTWAQ study of the Southern North Sea, Vos and Schuttelaar (1995) followed this strategy of using a linear relation. From a fit of NERC in-situ data for 1990 against weekly composites of Reflectance R(0+) they found that the saturation threshold is ~25 mg/l. Remote Sensing images from the NOAA/AVHRR satellite only render information on concentration gradients (i.e. on patterns) below this threshold concentration and show hardly any gradient above this threshold concentration.

## 2.3.6    Conversion of Reflection images to TSM concentrations using modelling

Reflectance values can be converted into TSM concentrations using in-situ data. Due to inaccuracies in the correction procedures for atmospheric disturbance and sea surface glint, every reflection image requires a different conversion, however. Therefore, the use of Remote Sensing images for the whole year would require an enormous amount of in-situ data.

In order to circumvent this conversion problem, Vos and Schuttelaar (RESTWAQ study, 1995) developed a procedure in which a traditionally calibrated water quality model can be used for conversion of Reflectance to TSM concentrations. This procedure proved to be successful. Spatial distributions of TSM were obtained from reflection imagery for the period February 1990 to December 1990.

The authors furthermore constructed monthly composites by averaging the available weekly composites. The use of monthly composites has the advantage that:

- much of the noise and the high small scale variability in the background of the images is eliminated;
- the patterns in the images are better comparable with the models, which aim at describing slow processes on time scales of months to years. The fast erosion and sedimentation processes that occur at time scales of hours are often difficult to interpret and not well represented by such water quality models.

## 3.    Available data and data assimilation procedure

### 3.1 Available fully processed Remote Sensing images

At Delft Hydraulics, the following weekly composites and daily images are available as the basis remote sensing data for use in the PROMISE sediment modelling:

- weekly composites of above-water Reflectance for 1990 (weeks 4 - 52, with week 13 missing), 1994 (weeks 9 - 40) and 1995 (weeks 9 - 52);
- a selection of 'best' daily images of above-water Reflectance for 1990: (22 days: 2/16, 3/16, 3/20, 4/1, 4/5, 4/6, 4/7, 4/14, 4/24, 4/25, 5/4, 5/5, 5/8, 5/26, 6/17, 7/12, 7/13, 8/2, 8/13, 8/28, 9/13, 10/12)
  and 1995 (29 days: 4/12, 4/21, 5/04, 5/21, 5/29, 5/30, 6/18, 6/27, 6/28, 7/08, 7/25, 7/26, 7/30, 7/31, 8/01, 8/02, 8/05, 8/10, 8/11, 8/12, 8/16, 8/17, 8/18, 8/19, 8/21, 8/22, 10/05, 10/09, and 10/24).

As an example, Figure 2 shows the weekly composite for week 1995/41.

Patterns in these best daily images are consistent with patterns observed in the weekly composite. However, the absolute level of Reflectance is very different for every image, and seems to be related very much to the sun-angle at the time of passage. Tidal effects can not be recognized in the daily images.

Weekly composites have been processed to monthly composites for 1990 (Feb-Dec), 1994 (March-Sept) and 1995 (March-Dec). The weekly and monthly composites form a smooth time-series of TSM data after conversion of Reflectance to TSM using model results (Vos and Schuttelaar, 1995). The following structures have been detected in these composites for all years studied (1990, 1994 and 1995):

1. Most images demonstrate relatively low reflectance before the Dutch Coast, although high concentrations are often found in a small thin zone directly along the coast. On the contrary, high reflectance values are found along the British Coast (Thames estuary, Suffolk Coast, Humber Estuary and Flamborough Head). Most often, also the Flemish Banks and the Wadden Sea show fairly high reflectance values, although generally lower values are found than for the British Coast.

2. In winter periods a plume of reflectance is recognized, that stretches from the coasts of Norfolk and Suffolk into the Southern North Sea. This phenomenon correlates with periods of high wind speeds from the south-west.

3. The most stable phenomenon in the reflectance pictures is the high reflectance in the Thames estuary. Patterns of TSM are found around the Isle of Wight in periods of high wind speeds from the south-west. These structures follow the coast of England and do not mix with TSM patterns that are found along the French coast.

A recently completed detailed study on TSM patterns in the Dutch Coastal Zone using independent data sets of 1994 and 1995 confirms the earlier observed clear structure: a narrow band of high TSM-concentrations goes from the Flemish Banks, along the Dutch Coast and the Dutch Wadden Sea. This band disappears almost completely in May, although TSM is still found in the region south of the Eastern Scheldt (Boon and Baart, 1996).

## 3.2 Data assimilation procedure

In their study, Vos and Schuttelaar (1995) proposed a formal procedure to assimilate patterns of TSM, obtained from Remote Sensing data, into a water quality model. This methodology for assimilating the calibrated RS images into the water quality model was subsequently further developed and tested. A quantitative norm or cost function was defined to measure the differences between model concentrations and remote sensing concentrations of TSM for a given number of geographic zones (in this case: 22) in the Southern North Sea. The cost function had to be both robust, i.e. not reacting strongly to noise (or other small scale fluctuations), as well as sensitive to adaptations in the relevant patterns of TSM. It was successfully evaluated in terms of these two criteria.

The cost function then indicates the North Sea zones and the periods in the year for which model results should be improved and adaptions in the model were required. In the following model calibration or 'optimization' step, adaptions to the model were made by means of model parameter adjustments. In the final step, the optimized model was validated against an independent set of available field data.

The advantage of such a cost function approach is that it gives reproducible results.

In summary, the methodology for integration of data from in-situ measurement, Remote Sensing and models involves the following 6 steps (Vos and Schuttelaar, 1995):

1)   Initial calibration of the water quality model for TSM based on sediment fluxes and correct mass balance;

2)   Scaling of the remote sensing data on the model results on the basis of weekly composites. The total mass in the model is used to scale the Remote Sensing reflectance imagery to Total Suspended Matter concentration (TSM in mg/l);

3)   Design and testing of a suitable cost function;

4)   Comparison of model results and Remote Sensing data of TSM in terms of the cost function, which gives a quantitative estimate of the agreement between model results and the Remote Sensing data. A smaller cost function implies better agreement;

5) Optimized calibration of the model by assimilation of Remote Sensing information of TSM into the model. This is done by iterative minimizing the cost function;

6) Validation of the optimized model and model results using available in-situ data.

The above integration of remote sensing data and water quality modelling resulted in a considerable improvement in the calibration of both remote sensing images and model concentrations of TSM (Vos and Schuttelaar, 1995). Using the model, the remote sensing reflection images can be scaled to a consistent time series of suspended matter data. At the same time, the patterns from the remote sensing images can be used to improve the model calibration, using the structured cost function approach.

The above approach forms the basis for the combination of the NOAA/AVHRR remote sensing images and the TSM modelling and model sensitivity analysis foreseen in PROMISE.

As a first step in PROMISE, the cost functions are being refined further. Amongst others, they will allow for the simultaneous assimilation of both Remote Sensing data and in-situ data in the water quality model. A second step is the automization of the calibration procedure, in which use is made of the adjoint formalism.

## 4. Summary and conclusions

*NOAA/AVHRR imagery and TSM*

NOAA/AVHRR Reflectance imagery, when corrected for atmospheric disturbance and sea surface glint, gives useful information on the spatial distribution of TSM in large marine systems. For regions close to the coast, satellite Remote Sensing can not be used since Reflectance in the weekly composites saturates at high (> 25mg/l) concentrations.

*The role of TSM*

Total Suspended Matter (TSM) strongly influences the clarity of the water column, and through this, various other water quality parameters, like Chlorophyll-a (and so nutrients), heavy metals and organic micropollutants. Reliable water quality models for TSM are an important means in the understanding not only of the behaviour of TSM, but of the transport of these other substances as well. As a consequence, the assimilation of Remote Sensing data into a water quality model for TSM can be essential for improvement of our understanding of the behaviour of water quality parameters which as such cannot be monitored with Remote Sensing.

*Availability of NOAA/AVHRR RS data*

For the years 1990, 1994 and 1995, 48, 31 and 43 weekly and 11, 7 and 10 monthly composites of thoroughly processed NOAA/AVHRR RS images are available. Our modelling in PROMISE will therefore focus on these periods and subperiods thereof.

*Available in-situ data*

Limited in-situ data are available for the same periods. Since the focus lies on the use of RS data, and in-situ data are not required for scaling the RS images, the available in-situ data is considered to be sufficient for the modelling foreseen in PROMISE.

*Scaling of RS imagery*

Using a water quality model for TSM to scale NOAA/AVHRR reflectance to TSM is a feasible and very useful procedure for the interpretation of Remote Sensing Imagery.

Since NOAA/AVHRR reflectance imagery is not multi-temporal valid, and since there is a lack of good in-situ data sets for calibration of RS imagery, this scaling procedure is in practice an essential step for a subsequent successful assimilation of Remote Sensing patterns into a water quality model.

*Formal data assimilation*

The integration of data into a water quality model should be based on validated structured and quantitative methods, since these satisfy the requirements of objectivity and reproducibility. Vos and Schuttelaar (1995) have demonstrated that monthly Remote Sensing composites for TSM can be assimilated successfully into a water quality model by means of minimization of a suitably chosen cost function. In PROMISE we aim at generalizing this methodology and automating it, using adjoint formalisms.

*TSM sensitivity studies*

With the above structured combination of both in-situ data and Remote Sensing data into water quality models using formal data assimilation procedures, water quality models are well suited to the study of TSM behaviour and the analysis of the influence of errors and uncertainties in the data, the model parameters and the model forcing, such as is undertaken in PROMISE. The optimized model describes the global sediment distribution in the water system.

**Acknowledgement**

## 5. References

Althuis, IJ.A. and S.Shimwell,
'*Interpretation of Remote Sensing Imagery for Suspended Matter Monitoring in Coastal Waters*',
Earsel Symposium 1994, Delft, The Netherlands.

Boon, J.G. and A.C. Baart,
'*Meetstrategie 2000+, Integratie van Remote Sensing, in-situ waarnemingen en modelberekeningen van zwevend stof in de Nederlandse kustzone*',
DELFT HYDRAULICS Report Z2066, November 1996.

Dekker, A.G.,
'Detection of optical water quality parameters for eutrophic waters by high resolution remote sensing',
Thesis, V.U. Amsterdam, 1993

Gerritsen, H. and R.J. Vos,
'Use of remote sensing products at Delft Hydraulics',
Remote Sensing Newsletter (BCRS), December 1996, 21-23

Gordon, H.R., Brown O.B. and M.M. Jacobs,
'Computed relationships between the inherent and apparent optical properties of a flat homogeneous ocean',
Applied Optics, 14, 1975, 417-427

Kirk, J.T.O,
'Volume scattering function, average cosines, and the underwater light field',
Limnol. Oceanogr. 36(3), 1991, 455-467

Krijgsman, J.,
' Optical remote sensing of water quality parameters; Interpretation of reflectance spectra', Thesis, University of Technology, Delft, 1994

Marees, G. and Wernand M.R.,
'Interpretation of optical remote sensing data over coastal waters',
BCRS report 91-27, Delft, 1992, 33-44.

Petzold, T.L.,
'Volume scattering functions for selected ocean waters',
University of California, San Diego: Scripps Inst. Oceanogr. Visibility Lab.,Ref.72-78, 1972.

Prangsma, G.J. and J.N. Roozekrans,
Int. J. Remote Sensing Vol.10, p. 811, 1989.

Prangsma, G.J. and J.N. Roozekrans,
'Ontvangst van het aard-atmosfeersysteem door de NOAA-satellieten (ontvangst, productie, toepassing en gebruik van de NOAA-data)',
BCRS report 92-025, Delft, 1992.

Prieur, L. and S. Satheyndrath,
'An optical classification of coastal and oceanic waters based on the specific absorption curves of phytoplankton pigments, dissolved organic matter and other particulate material',
Limnol. Oceanogr. 26, 1981, 671-689

Schuttelaar, M.,
'Application of Remote Sensing to the modelling of suspended matter transport in the North Sea',
(Report for DEA National d'Hydrologie at ENGREF, Paris France), DELFT HYDRAULICS, September 1995.

Stumpf, R.P.,
'*Remote Sensing of Water Clarity ad Suspended Sediments in Coastal waters*',
ERIM Symposium June 1992, USA, Session 3 and B, (Water Quality), 293-305.


Viollier, M., Tanré, D. and P.Y. Deschamps,
'*An algorithm for Remote Sensing of water color from space*',
Boundary-layer metereology 18, (1980), 247-267;


Vos, R.J.,
' RESTWAQ: *Applications of Remote Sensing to Water Quality Modelling (Data assessment and development of methodology)*',
DELFT HYDRAULICS report T1083/T1479, March 1995;


Vos, R.J. and M. Schuttelaar,
'RESTWAQ, *Data asssessment, data-model integration and application to the Southern North Sea*',
BCRS Report 95-19, Delft, 1995.


Vos, R.J. and M. Schuttelaar,
'*An integrated data-model system to support monitoring and assessment of marine systems*',
First International Conference on EuroGOOS, 7-11 October 1996, The Hague, The Netherlands.

REFLECTIE
NOAA-14 opname
Datum: 28- 6-95
Tijd: 12:35 GMT
Res.: 1.00 km

WOLK

LAND

0.00 %

0.25

0.50

0.75

1.00

1.25

1.50

2.00

2.50

REFLECTIE
COMPOSIET van
18 NOAA-beelden
PERIODE:
 9-10-95 10 GMT
15-10-95 13 GMT

WOLK

LAND

0.00 %

0.25

0.50

0.75

1.00

1.25

1.50

2.00

2.50

© KNMI
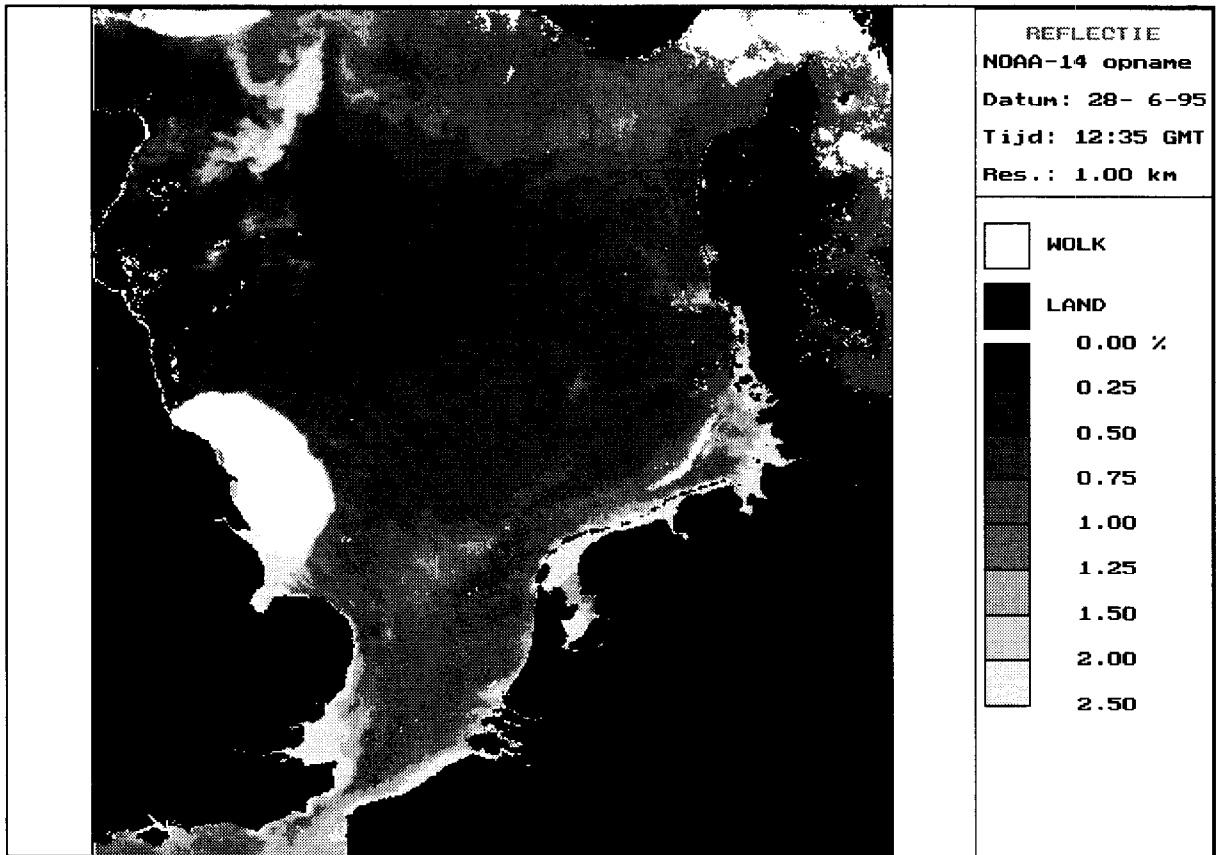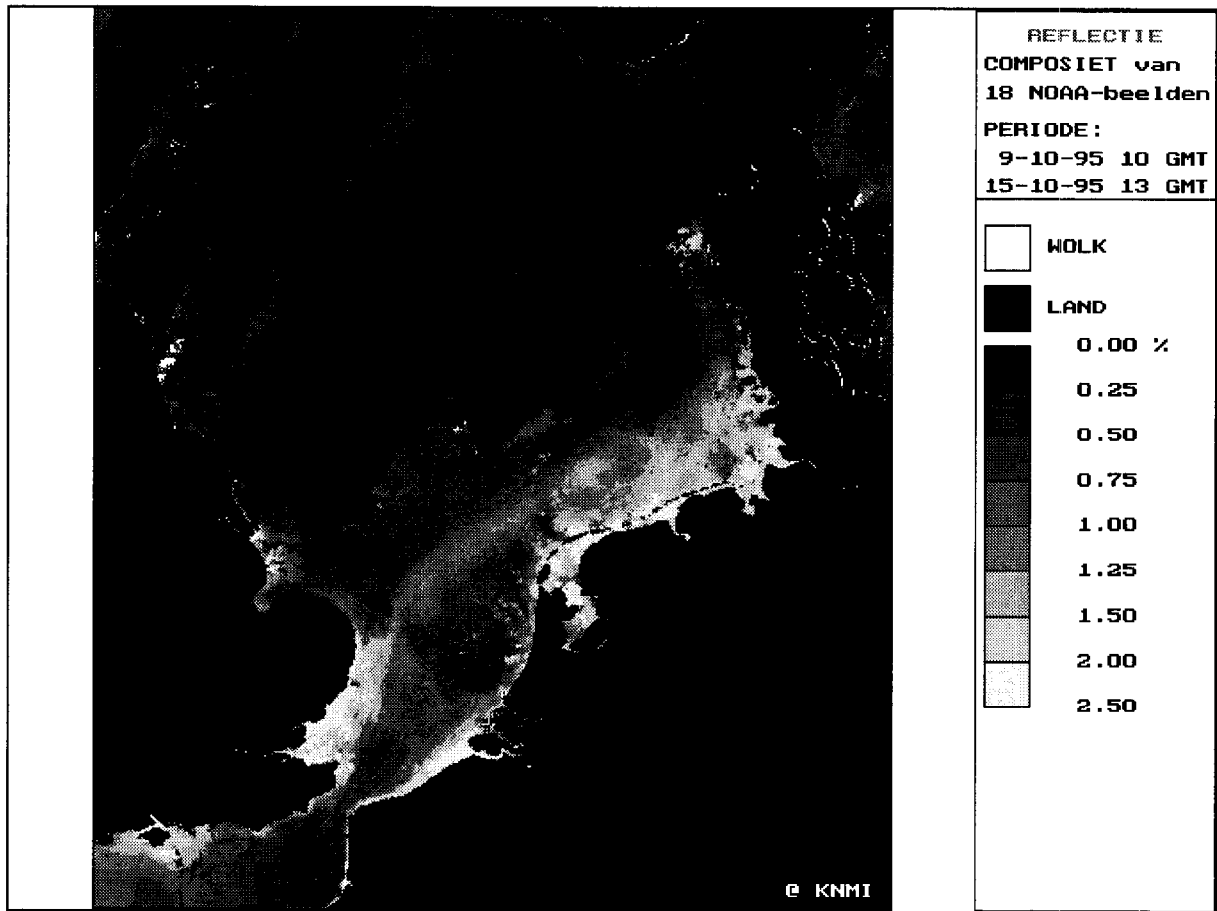
# Appendix C: Data assimilation in a EuroGOOS framework

# DATA ASSIMILATION IN A EUROGOOS FRAMEWORK

by

Paul G.J. ten Brummelhuis [1],

Geir Evensen[2],

Herman Gerritsen[1]

[1]:     Delft Hydraulics, Delft, The Netherlands

[2]:     Nansen Environmental and Remote Sensing Center, Bergen, Norway

December, 1996

## ACKNOWLEDGEMENT

## INTRODUCTION

The purpose of this section is to identify the role of data assimilation under EUROGOOS. EUROGOOS has identified the need for developing and implementing operational marine monitoring and prediction systems for the European coastal zone. Such systems must include both observations from the environmental satellites and in-situ observations collected from buoys deployed in the ocean in addition to the use of numerical prediction models. Integrated use of observations and models can only be done in a consistent way through the use of data assimilation procedures. Here, a brief overview is given of the current status of data assimilation developments and their applications. This note may form the basis for further developments and applications to be planned and executed within EUROGOOS.

## BACKGROUND

Information about numerous physical processes can be provided by numerical models and observed data. A considerable step ahead can be made by exploiting the complementary character of models and observations: the generic, qualitative character of process knowledge embedded in models versus the specific, quantitative character of observed data. By means of data assimilation, model information and observed information can be integrated in an optimal way, taking into account the uncertainties in the model and the observations. This provides a framework to:

\*    determine accurate representations of the model state in space and time, e.g. to be used as initial conditions in forecast runs,
\*    improve monitoring capabilities,
\*    to validate and calibrate the models against observations from prototype,
\*    provide error estimates on monitoring and forecast products.

Data assimilation will indeed play an important role within the future EUROGOOS plans and activities. Clearly, without consistent data assimilation procedures, every numerical model will drift away from the observed state and the model results will be worthless for prediction purposes. Indeed, in numerical weather prediction one has acknowledged that further improvement of the forecasts may be better achieved by improving the data assimilation procedures than the quality of the atmospheric models.

## BASIC PRINCIPLES

The main objective of an information system with numerical models, observations and data assimilations as components is to improve the knowledge of a dynamical system, by extracting a maximum amount of information from both model and observations, and combine this information in an optimal way.  This involves the use of information from a limited set of observations, which are directly or indirectly related to the model state, to 'control' the model state, the model forcing and/or model coefficients.

The general formulation of the data assimilation problem, both for linear and nonlinear models is now well understood [Bennett (1992), Evensen (in press)]. The bottom line is that, in allowing for model errors (that is errors in the model equations, the initial and boundary conditions) and observation errors, the assimilation objective is to minimize these errors in a least square sense.

The method adopted for a particular application will usually depend on aspects like the nonlinearity of the system, the length of the assimilation interval, the dimension of the model state and the overall objective of the assimilation system [for examples, see the special issue of Tellus 45A (5), 1993].

The advantage of (computationally demanding) model-based assimilation techniques such as Kalman filtering or the adjoint method, is that the updated model state (after assimilation) is consistent with the model dynamics. However, the effectiveness of the assimilation depends on the accuracy the specification of the statistics of the model and data uncertainties. This strongly emphasizes the need for validation of the models as well as the data that are to be assimilated.

## APPLICABILITY AND EXPERIENCE

The development of operational data assimilation is strongly stimulated by the needs of numerical weather prediction [Talagrand and Courtier (1987)]. The last decade also applications in operational storm surge prediction [Heemink and Kloosterhuis (1990), Bolding (1995)] and (ocean) wave prediction [Calkoen et. al. (1995)] have been realized. These applications are all made possible by the readily available data from buoys and satellites.

In oceanography, as well as in meteorology, various types of data are available for assimilation (e.g. sea surface height, temperature and salinity in oceanography). The limits of using simplistic assimilation schemes that are based on ad hoc procedures to determine the error statistics of the

predicted model state become apparent in the form of problems regarding the transfer of surface observations over the vertical and the lack of consistency between, e.g., the temperature and salinity properties after assimilation [Malanotte-Rizzoli and Young (1995)]. Therefore, there is a significant ongoing effort in implementing and validating the more advanced assimilation schemes where realistic error statistics are taken into account.

In coastal morphology, the potential of data assimilation is also recognized.
The assimilation of selected data in coastal morphological models is not only focused on the estimation of the current morphological state but is also intended to increase our knowledge of the morphodynamic processes in the coastal zone.

As for the assimilation of data in ecosystem models, only a few applications have been reported [Prunet et al. (1996)]. The data assimilation problem for 3-D ecosystem dynamics has not been properly adressed so far. However, the need for data assimilation in an ecosystem context is obviously required for future operational ocean information systems.

## KEY ISSUES

The key issues wrt. the optimal integration of model and observational information that need to be adressed considering their relevance to EUROGOOS' objectives are:

* A proper analysis of the error statistics of assimilation products. This is necessary in order to evaluate the impact of individual observations, to develop computationally efficient optimal interpolation schemes that can be used in an operational context and to improve the consistency of the assimilation procedure and the model dynamics.

* Over the last few years, the amount of field data is rapidly growing, especially RS data. These RS data have contributed significantly because of the high spatial correlation of the data (patterns), despite its low temporal coverage and sometimes limited accuracy, as opposed to in-situ data. At this moment there is a need to evaluate the complementarity of in-situ and RS data, both in the assimilation process and in the pre-operationalization of observation systems: there is a need to identify in advance what kind of (and how) parameters need to be measured.

* The required amount of information of observations and their capability of controlling the model state must be evaluated. Currently the most promising remote sensing observations for use in OGCMs are the radar altimeter and sea surface temperature data, which probably provide enough information to control the surface circulation. The usefulness of additional hydrographic in-situ observations must be examined.
For marine ecosystem models there is significantly less data available. Ocean colour data, e.g. OCTS (Ocean Colour and Temperature Scanner) data from the ADEOS-1, are likely to be useful for controlling the phytoplankton concentrations in the ocean, but very little information is available regarding variables like zoo-plankton and nitrates.

* Further work is needed wrt. the mapping from observations to the model variables, e.g. the mapping of observed remote sensing reflection images to concentrations of suspended matter. One must be careful not to introduce unphysical biases by specifying improper relations between the data and the model variables. Moreover, the appropriate temporal and spatial scales and the resolution must be determined that allow to extract meaningful information from the differences between the modeled and the observed parameters.

## SUMMARY

* A future operational coastal ocean and environmental information system must bc built on systematic integration of remote sensing observations, in-situ observations and numerical models. Givcn models and observations, data assimilation modules (being the interface between them) are the third essential component of information systems,

* Assessment of models and observations should be made to identify their role in integrated (information) systems and to address questions like cost-effectiveness.

* A prerequisite for assimilation of observational data is the availability of digital, well-documented, easily accessible data, which have been screened by (standardized) QC procedures.

Based on the potential of data assimilation and the objectives of EUROGOOS, new initiatives should be formulated that build upon the notions mentioned in the previous section.

## REFERENCES

Bennett, A.F.,
*Inverse methods in physical oceanography,*
Cambridge University Press, 1992.

Bolding, K.,
*Results from a semi operational storm surge warning system using a stationary Kalman filter,*
in: Computer modelling of seas and coastal regions, ed. by C.A. Brebbia, L. Traversoni and L.C. Wrobel, pp. 309-318, Computational Mechanics Publications, Southampton Boston, 1995.

Calkoen, C.J., G.J. Wensink, M. Naeije and E. Boorsma,
*A global wave climate information system based on satellite altimeter observations,*
BCRS report no. 95-04, 1995.

Heemink, A.W. and H. Kloosterhuis,
*Data assimilation for non-linear tidal models,*
Int. J. for Num. Methods in Fluids, vol. 11, pp. 1097-1112, 1990.

Malanottc-Rizzoli, P. and R.E. Young,
*Assimilation of global versus local data sets into a regional model of the Gulf Stream system,*
in: Journal of geophysical research, vol. 100 (24), pp. 773-796, 1995.

Prunet, P., J.-F. Minster, V. Echevin and I. Dadou,
*Assimilation of surface data in a one-dimensional physical-biogeochemical model of the surface ocean (2). Adjusting a simple trophic model to chorofyll, temperature, nitrate an pCO2 data,*
in: Global biogeochemical cycles, vol 10 (1), pp. 139-158, 1996.

Talagrand, O. and P. Courtier,
*Variational assimilation of meteorological observations with the adjoint vorticity equation. I: theory,*
Q.J.R. Meteorological Society, vol. 113, pp. 1311-1328, 1987.